BSPE 9830R-2087-5

시공간 변화에 따른 해저열수활동의 다양성 연구시스템구축

2009. 7

한 국 해 양 연 구 원

제 출 문

한국해양연구원장 귀하

본 보고서를 “한국해양연구원 창의과제 사업(08년도)”의 최종보고서로 제출합니다.

2009. 7

연구기관명: 한국해양연구원
연구책임자: 김종욱
참여연구원: 김정훈, 손주원
연 구 조 원: 김아영

목 차

Chapter I. 기획연구

시공간 변화에 따른 해저열수활동의 다양성
연구 시스템 구축

1. 추진 필요성 및 목적

1.1. 추진 필요성

추진필요성

□ 해저열수활동은 해양과 지구내부(지각, 맨틀) 사이의 물질 및 에너지 교환의 장으로 물리/화학/지질/생물 등 지구과학의 전분야가 융합된 거대과학의 연구토대를 제공하지만 국내의 관련 연구는 열수활동의 결과물인 해저열수광상의 자원 개발에 치중되어 있음

□ 해저열수활동은 판구조론이 정립됨에 따라 그 존재를 예측하여 발견한 인류 과학사의 큰 성과임. 하지만, 열수분출구 주변의 화학합성에 의한 생태계의 존재는 전혀 예상하지 못했던 결과였음

□ 해저열수활동은 중앙해령, 후열도확장대, 열도화산대 등 매우 상이한 지질환경 공간에서 다양한 형태로 존재하고 있으며, 이러한 다양성은 열수활동의 결과물인 해저열수광상의 조성과 규모에 영향을 미치는 동시에 열수주변에 형성되는 생물다양성에도 영향을 미침

□ 현재 알려진 활동성 열수분출구의 연대는 수십 년에서 수만 년으로 다양하며, 열수분출의 생성주기 또한 생성지역에 따라 차이가 큰 것으로 파악됨. 하지만, 열수분출의 중지와 소멸에 따른 분출구의 변화(변질작용, 생물군 변화 등)는 아직 잘 알려져 있지 않음

□ 해저열수활동이 화산활동에 수반됨을 감안할 때 과거의 열수작용에 의해 생성된 열수분출지역(extinct vent)은 활동성 열수지역에 비해 더 많이 분포하고 있을 것으로 예측되나 그 탐지기술은 아직 초기단계에 머물러 있으며, 원격탐사 기술이 주로 사용될 수 있을 것으로 예측되고 있음

□ 시공간에 따른 해저열수활동 다양성 연구는 주로 활동성 지역에 한정되어 있는 해저열수분출 연구의 공간을 비활동성 지역으로 확대할 수 있는 토대를 마련하며, 이는 열수분출 및 그 구성요소의 진화에 대한 이해의 폭을 넓히는 한편, 열수생태계라는 중요한 환경에 대한 피해를 최소화하면서 해저열수광상을 개발에도 활용될 것임

○ 해저열수분출은 대륙열곡, 중앙해령 확장대 및 주변해저산, 열점, 열도화산대, 후열도분지 확장대 및 열곡대 등 다양한 지구조 공간에서 생성됨

○ 열수분출의 발견이후 수행된 대부분의 연구는 활동성 지역에 집중되었으며, 비활동성 및 소멸지역에 대한 연구는 아직 초기단계에 머물러 있음

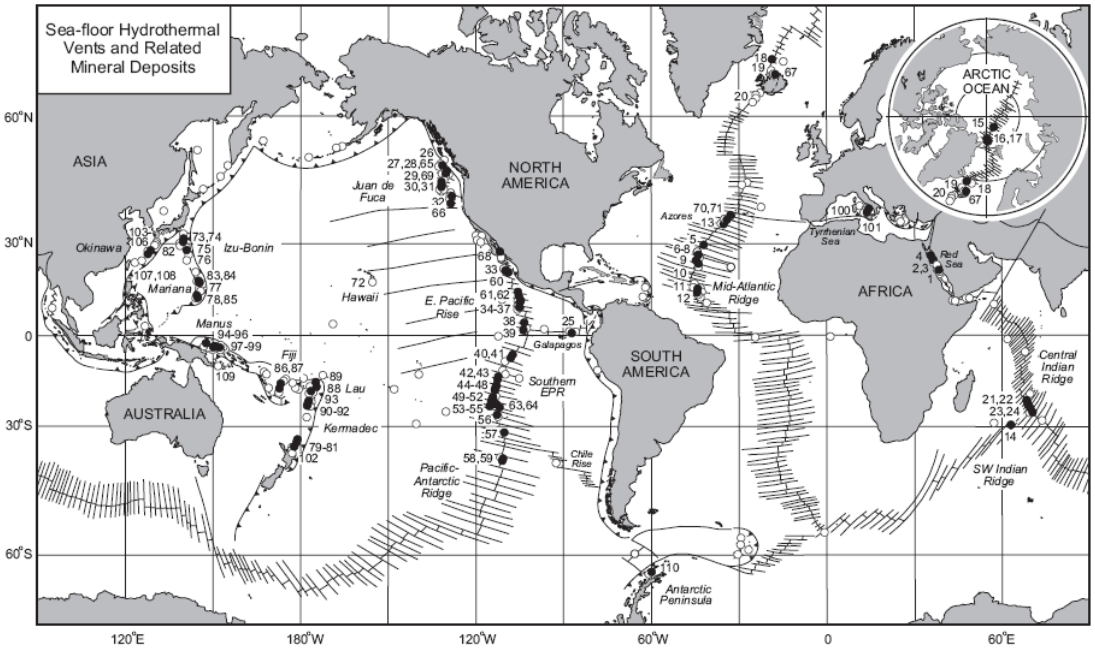

Intracontinental rifts
1. Atlantis II Deep, Red Sea
2. Thetis, Nereus, Gypsum Deeps
3. Kebrit Deep, Red Sea
4. Shaban Deep, Red Sea

Slow-spreading mid-ocean ridges
5. Broken Spur, Mid-Atlantic Ridge
6. TAG Mound, Mid-Atlantic Ridge
7. MIR Zone, Mid-Atlantic Ridge
8. Alvin Zone, Mid-Atlantic Ridge
9. 24°30'N, Mid-Atlantic Ridge
10. Snakepit Field, Mid-Atlantic Ridge
11. 15°N, Mid-Atlantic Ridge
12. Logatchev Field, Mid-Atlantic Ridge
13. Rainbow Field, Mid-Atlantic Ridge
14. Mt. Jourdanne, Southwest Indian Ridge
15. Gakkel Ridge, Arctic Ocean
16. Aurora Field, Arctic Ocean
17. Lena Trough, N. Mid-Atlantic Ridge
18. N. Kolbeinsey Ridge
19. Kolbeinsey Ridge
20. Reykjanes Ridge

Intermediate-rate mid-ocean ridges
21. JX/MESO Zone, Central Indian Ridge
22. EX/FX Zone, Central Indian Ridge
23. Kairei Field, Central Indian Ridge
24. Edmond Field, Central Indian Ridge
25. Galapagos Rift
26. S. Explorer Ridge
27. High-Rise, Endeavour Ridge
28. Main Field, Endeavour Ridge
29. CoAxial Site, Juan de Fuca Ridge
30. North Cleft, Juan de Fuca Ridge
31. South Cleft, Juan de Fuca Ridge
32. North Gorda Ridge

Fast-spreading mid-ocean ridges
33. 21°N, Northern EPR
34. 12°50'N, Northern EPR
35. 11°32'N, EPR Seamount
36. 11°N, Northern EPR
37. 9-10°N, Northern EPR
38. 3°55'N, Northern EPR
39. 1°44'N, AHA Field, EPR
40. 7°00'S, Southern EPR
41. 7°30'S, Southern EPR
42. 14°00'S, Southern EPR
43. 15°00'S, Southern EPR
44. 16°40'S, Southern EPR
45. 17°27'S, Southern EPR
46. 17°30'S, Southern EPR
47. 18°10'S, Southern EPR
48. 18°26'S, Southern EPR
49. 20°00'S, Southern EPR
50. 20°50'S, Southern EPR
51. 21°30'S, Southern EPR
52. 21°50'S, Southern EPR
53. 22°30'S, Southern EPR
54. 22°58'S, Southern EPR
55. 23°30'S, Southern EPR
56. 26°10'S, Southern EPR
57 31°51'S, Southern EPR
58. 37°40'S, Pacific-Antarctic Ridge
59. 37°48'S, Pacific-Antarctic Ridge

Off-axis volcanoes
60. Green Seamount
61. 14°N, Northern EPR
62. 13°N, Northern EPR
63. 23°19'S, Southern EPR
64. Pito Seamount

Sedimented ridges and related rifts
65. Middle Valley
66. Escanaba Trough
67. Grimsey Field
68. Guaymas Basin

Ridge-hotspot intersections
69. Axial Seamount, Juan de Fuca Ridge
70. Lucky Strike, Azores
71. Menez Gwen, Azores

Intraplate volcano
72. Loihi Seamount, Hawaii

Intraoceanic arcs
73. Kita Bayonnaise, Izu-Bonin Arc
74. Myonjinsho, Izu-Bonin Arc
75. Suiyo Seamount, Izu-Bonin Arc
76. Kaikata Seamount, Izu-Bonin Arc
77. East Diamante, Mariana Arc
78. Forecast Field, Mariana Arc
79. Clark Seamount, Kermadec Arc
80. Rumble II West, Kermadec Arc
81. Brothers, Kermadec Arc

Intraoceanic back-arc basins
82 Sumisu Rift, Izu-Bonin Arc
83. Alice Springs, Mariana Trough
84. Central Mariana Trough
85. Southern Mariana Trough
86. White Lady, North Fiji Basin
87. Père Lachaise, North Fiji Basin
88. Papatua Site, Northern Lau Basin
89. Kings Triple Junction, Northern Lau
90. White Church, Southern Lau Basin
91. Vai Lili Field, Southern Lau Basin
92. Hine Hina, Southern Lau Basin
93. Central Lau Basin
94. Central Manus Basin
95. Vienna Woods, Manus Basin
96. Western Ridge, Manus Basin

Transitional island arcs and back-arc rifts
97. Pacmanus, E. Manus Basin
98. SuSu Knolls, E. Manus Basin
99. Desmos Cauldron, E. Manus Basin
100. Palinuro Seamount, Tyrrhenian Sea
101. Panarea Seamount, Tyrrhenian Sea
102. Calypso Vents, Taupo Zone

Intracontinental back-arc rifts
103. Minami-Ensei, Okinawa Trough
104. North Iheya, Okinawa Trough
105. Clam Site, Okinawa Trough
106. Izena Cauldron, Okinawa Trough
107. Hatoma Knoll, S. Okinawa Trough
108. Yonaguni Knoll, S. Okinawa Trough

Volcanic rifted margins
109. Franklin Seamount, Woodlark Basin
110. Bransfield Strait, Antarctica

Fig. 1. 기존에 발견된 해저열수 분출지역의 분포 및 생성환경에 따른 분류 (After Hannington and Monecke, 2006)

○ 해수와 해양지각의 반응에 의해 형성되는 해저열수활동은 1) 해양지각의 조성을 변화시키고, 2) 해수의 조성에 영향을 끼치며, 3) 금속광상을 형성하고, 4) 심해 생물군에 에너지를 공급하는 역할을 수행함

○ 다양한 환경에서 생성되는 열수의 조성은 주변 암의 조성, 마그마기원 휘발성물질의 공급, 기반암 내 구조(투수율), 열원의 외형과 속성, 온도, 압력 등 다양한 요인에 의해 달라짐

Table 1. 다른 지구조 환경에 분포하는 열수의 조성 (After Tivey, 2007)

	Mid-Ocean Ridge	Back-Arc	Rainbow	Lost City	Sediment-Hosted	Seawater
T (°C)	≤ 405	278 - 34	365	≤ 91	100 - 15	2
pH (25°C)	2.8 - 4.5	< 1 - 5.0	2.8	10 - 11	5.1 - 5.9	8
Cl, mmol/kg	30.5 - 1245	255 - 790	750	548	412 - 668	545
Na, mmol/kg	10.6 - 983	210 - 590	553	479 - 485	315 - 560	464
Ca, mmol/kg	4.02 - 109	6.5 - 89	67	< 30	160 - 257	10.2
K, mmol/kg	-1.17 - 58.7	10.5 - 79	20	-	13.5 - 49.2	10.1
Ba, µmol/kg	1.64 - 18.6	5.9 - 100	> 67	-	> 12	0.14
H_2S, mmol/kg	0 - 19.5	1.3 - 13.1	1	< 0.064	1.10 - 5.98	-
H_2, mmol/kg	0.0005 - 38	0.035 - 0.5	13	< 1 - 15	-	-
CO_2, mmol/kg	3.56 - 39.9	14.4 - 200	na	bdl	-	2.36
CH_4, mmol/kg	0.007 - 2.58	.005 - 0.06	0.13 - 2.2	1 - 2	-	-
NH_3, mmol/kg	< 0.65	-	-	-	5.6 - 15.6	-
Fe, µmol/kg	7 - 18700	13 - 2500	24000	-	0 - 180	-
Mn, µmol/kg	59 - 3300	12 - 7100	2250	-	10 - 236	-
Cu, µmol/kg	0 - 150	.003 - 34	140	-	<0.02 - 1.1	-
Zn, µmol/kg	0 - 780	7.6 - 3000	160	-	0.1 - 40.0	-
Pb, µmol/kg	0.183 - 0.1630	0.036 - 3.900	0.148	-	<0.02 - 0.652	-
Co, µmol/kg	0.02 - 1.43	-	13	-	< 0.005	-
Cd, µmol/kg	0 - 0.910	-	0.130	-	<0.01 - 0.046	-
Ni, µmol/kg	-	-	3	-	-	-
SO_4, mmol/kg	0	0	0	1 - 4	0	28
Mg, mmol/kg	0	0	0	< 1	0	53

○ 뜨거운 열수가 차가운 해수로 분출하면서 주로 금속 황화광물로 이루어진 열수광체가 형성되며, 이때 이들 광체의 크기는 수 m에서 수백 m의 크기로 다양함

○ 열수광체의 크기, 형태, 조성에 영향을 미치는 요인은 열수의 조성, 열수와 해수가 혼합되는 방식, 열수분출의 지속성 등이 있으며, 이는 열수활동이 생성되는 지구조 환경과도 매우 관련됨

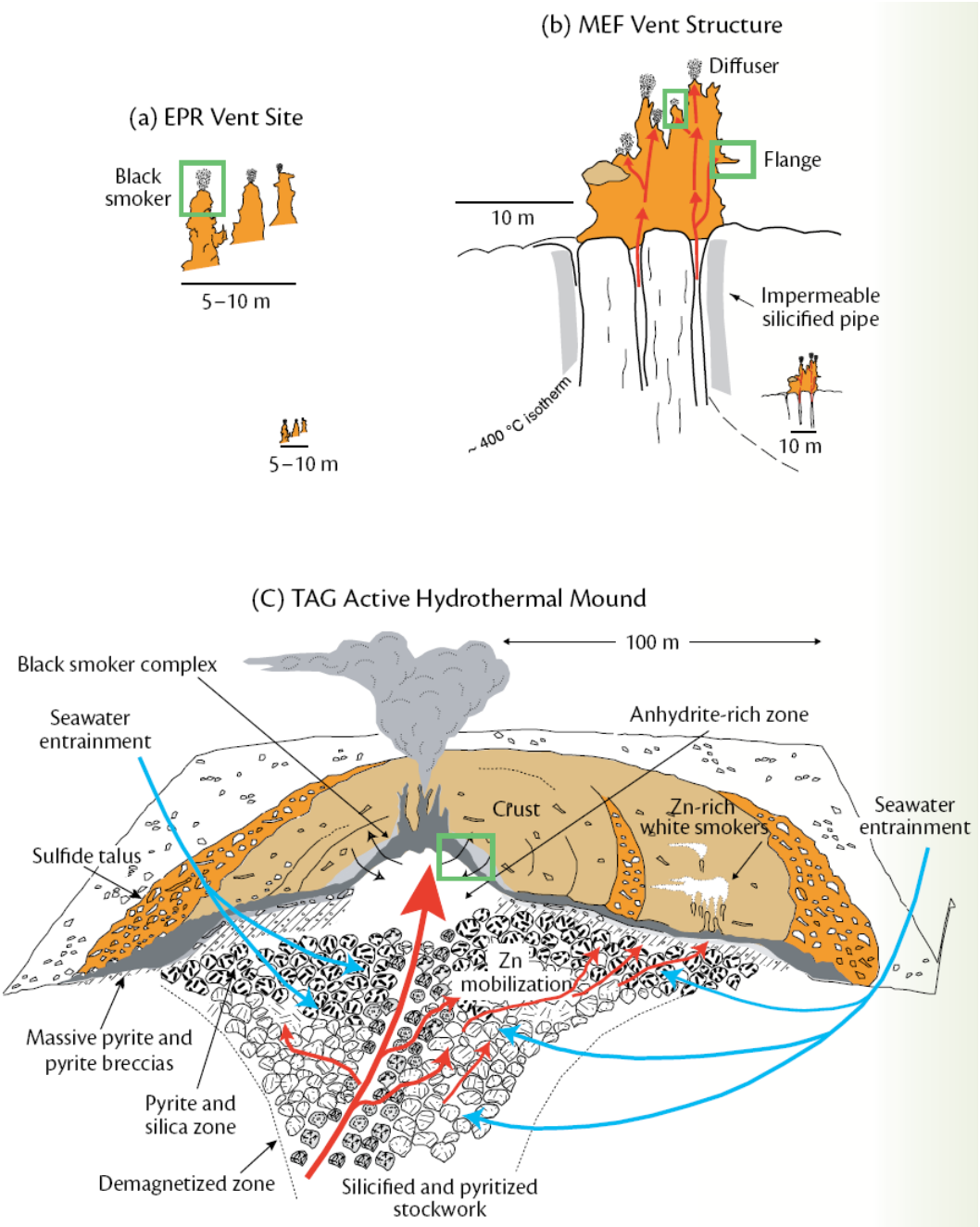

Fig. 2. 다양한 크기와 형태의 열수광체(After Tivey, 2007)

○ 열수분출구 주변에 서식하는 생물군집의 연구가 축적됨에 따라 서로 다른 지역의 열수분출구에는 각각의 독특한 생물군집이 발달하고 있음이 알려졌으나, 이들의 생물다양성과 분포특성은 아직 제한적으로만 이해되고 있으며, 현재 서로 다른 지역을 연결하는 퍼즐조각에 해당되는 지역에 대한 연구들이 추진되고 있음

Table 2. 열수 지역 별 우점 생물군집 (After Ramirez-Llodra et al, 2007)

Biogeographical Province and Depth	Dominating Fauna
Azores (shallow north Atlantic, 800-1700 m)	Bathymodiolid mussels, amphipods, and caridean shrimp
Mid-Atlantic Ridge between Azores Triple Junction and Equator (deep north Atlantic 2500-3650 m)	Caridean shrimp－ainly Rimicaris exoculata－and bathymodiolid mussels
South Mid-Atlantic Ridge	Caridean shrimp, bathymodiolid mussels, and clams
East Pacific Rise and Galapagos Rift	Vestimentiferan tubeworms － mainly Riftia pachyptila － and bathymodiolid mussels, vesicomyid clams, alvinellid polychaetes, amphipods, and crabs
Northeast Pacific	Vestimentiferan tubeworms excluding Riftiidae, polychaetes, and gastropods
Western Pacific	Barnacles, limpets, bathymodiolid mussels, “hairy” gastropod, vesicomyid clams, and shrimp
Central Indian Ridge	Caridean shrimp Rimicaris kairei, and mussels, “scaly” gastropods, and anemones

○ 화학합성이라는 매우 독특한 열수생태계의 존재는 해저열수분출에 의해 생성되는 금속광상의 자원개발을 제한하는 요인으로 작용함. 따라서 자원개발 후보지역은 이들 생물활동이 약해지거나 소멸된 비활동성/소멸성 분출지역을 대상으로 이루어질 것이나 아직 이들 비활동성 지역에 대한 과학적 이해가 부족함

1.2. 목적

목적

□ **열수분출구의 진화시기에 따른 지질, 화학, 생물 작용을 이해하고 특히, 열수활동 소멸 이후 진행되는 분출구 주변 특성의 변화를 파악함**
□ **해저열수활동이 생성되는 지구조환경 특성을 이해하고 열수작용의 조성 및 규모에 영향을 미치는 요인을 이해함**

□ **열수분출구의 진화시기에 따른 지질, 화학, 생물 작용을 이해하고 특히, 열수활동 소멸 이후 진행되는 분출구 주변 특성의 변화를 파악함**

○ 활동성 및 비활동성 열수분출지역 탐사기법 개발
○ 최신 동위원소 기법을 이용한 열수분출대의 연대측정
○ 열수분출지역의 활동성을 판별하기 위한 지질/화학/생물학적 기준 개발
○ 비활동성 열수분출대의 지질/생물 특성 파악
○ 비활동성 및 소멸성 열수분출대의 풍화/변질 결과 해석을 통한 열수광체 보존여부 및 자원가치 평가

□ **해저열수활동이 생성되는 지구조환경 특성을 이해하고 열수작용의 조성 및 규모에 영향을 미치는 요인을 이해함**

○ 열수분출지역의 지구물리/기반암 해석을 통한 지구조 특성 해석
○ 열수분출대의 조성 및 규모 조절인자 판별
○ 기존의 열수분출지역이 분포하는 지구조환경, 열수분출 특성, 열수 및 열수광체의 조성을 파악하고 지역적 특성을 평가

2. 국내외 연구개발 동향·분석

2.1. 관련 연구/기술의 국내외 동향

국외 동향

◇ 지난 1970년대 말 유인잠수정 Alvin을 이용하여 동태평양해령과 갈라파고스해령에서 해저열수분출이 확인된 이후, 해저열수시스템은 대양과 지구내부의 물질·에너지 순환, 지구상 생명의 기원 등의 거대담론을 밝혀내기 위한 유일한 연결고리로서의 학문적 관심과 육상에서 발견되는 금속광상을 형성한 근원지로서의 자원 경제적 관심을 동시에 불러와 현재까지 전 세계적인 탐사를 통해 250개 이상의 열수활동 지역이 확인되어 활발한 연구가 이루어지고 있음

◇ 이들 해저열수시스템 연구는 해양지질학, 해양지구물리, 해양물리, 해양화학, 해양생물, 탐사기술 등 종합적이고 다학제적인 연구를 요구함에 따라 미국, EU, 일본 등 선진국들은 Ridge2000, Ring of Fire, IODP, Interidge 등 다양한 국제공동연구 프로젝트를 통해 연구 활동이 이루어짐

◇ ChEss, CoML, SCOR 등의 연구프로그램을 통한 열수생태환경 연구는 열수활동에 의한 다양한 생물발생 경로와 규모를 파악하고 이들 생태계가 전 대양의 탄소순환에서 차지하는 역할을 정량적으로 규명하려는 단계로 발전되고 있음

◇ 최근 외국 민간 기업에 의한 해저열수광상의 자원개발 움직임이 활발해짐에 따라 InterRidge는 2008년 “Seafloor Mineralization" Working Group을 구성하여 해양광물자원 개발 시대를 대비한 해당분야 전문가 연구그룹을 조직하였음

국내 동향

◇ 국내의 해저열수활동 연구는 한국해양연구원의 기관고유 사업으로 1998-2000년 얍해구, 마누스분지, 우드락분지 지역의 탐사를 통해 처음 시작되었으며, 2001년부터 해양수산부의 연구개발과제인 남서태평양 광물자원 개발을 통해 북피지분지와 라우분지를 대상으로 주로 자원개발 목적의 연구를 수행해오고 있음

◇ 2006과 2007년에는 한국해양연구원에서 수행된 대양사업(POSEIDON)의 일환으로 마리아나열도의 해저산을 대상으로 열수환경 연구가 수행되어 열수분출을 확인하는 성과를 거두었으나 구체적이며 체계적인 분야별 연구수행은 진행되지 못하고 중단된 상태임

◇ 2004년부터 수행된 라우분지에서의 열수탐사를 통해 북동라우분지의 활동성 확장대인 FRSC와 NELSC, 활동성칼데라인 MTJ-1 지역에서 열수분출 근원지를 새로이 발견하는 성과를 거두었음

◇ 2008년 통가해역의 해저열수광상을 대상으로 3년간의 독점탐사권을 획득하였고 이를 바탕으로 해저열수광상개발사업단이 발족하여 본격적인 자원개발사업이 시작되었으며, 국제해저기구의 공해상 해저열수광상 탐사규칙 제정 움직임에 따라 인도양해령 등 공해상 해저열수광상 탐사를 준비 중임

◇ 국내의 해저열수활동 연구는 자원개발 목적의 일부분야에만 한정되어 왔으며, 남서태평양 도서국 EEZ에서 본격적인 자원개발 체제를 갖추고 인도양해령 등 공해상으로 그 범위를 확대하는 등 소기의 성과를 거두고 있음

◇ 하지만, 지구조/해저화산활동 해석, 열수플럭스, 열수생태 및 생물다양성연구 등 해저열수활동 연구의 주요 분야에 대한 접근은 매우 제약되어 있는 상태로 일부 연구자들의 개별연구 혹은 국제공동연구에 의존하고 있는 상태임

2.2. 관련기술의 시장규모 및 적용가능 분야

가. 관련기술의 시장규모

◇ 이 연구는 직접적으로 시장가치를 창출하는데 이용될 수 있는 기술개발 목적의 연구는 아님

◇ 하지만, 이 연구의 기대성과 중 하나는 해저열수분출이라는 극한지역에 대한 최신 해양탐사기술을 적용함으로써 관련 해양조선산업, 특히 자율형 수중탐사체를 이용한 원격탐사 시스템의 구축은 해양조사 장비관련 산업의 발전에 공헌할 것임

◇ 또한, 이 사업의 주요 목표 중 하나는 과거에 형성된 열수분출대의 보존가능성과 탐지가능성을 평가하는 것으로 실제로 과거 지질시대에 형성되어온 해저열수광체가 확장대 측면에 보존되어 있음이 확인될 경우, 해저열수광상 개발과 관련한 사업에는 상당한 파급효과가 있을 것임

나. 관련기술의 적용가능 분야

기술분류	적용 가능 분야
해양탐사기술	○ 근접해저면 탐사기술 ○ 기반암 및 열수변질대 연대측정기술 ○ 대양저 해저면 및 천부지층 내 자원 탐지 기술

2.3. 국내 연구개발 현황 및 능력분석

◇ 국내의 해저열수활동 연구는 지난 1998년 한국해양연구원의 기관고유 사업으로 시작되어 국가연구개발사업으로 약 10년에 걸친 연구경험을 토대로 기존에 알려진 지역의 탐사수행단계에서 독자적인 활동성 플룸 및 열수분출지역 추적이 가능한 탐사수행 능력을 갖춤

◇ 하지만, 원활한 대양탐사 수행을 위한 대형조사선 및 극한지역 탐사를 위한 유/무인 잠수정의 활용, 열수분출수 및 생물 채취 기술, AUV를 이용한 원격제어탐사기술의 도입은 해양과학기술 선진국들에 비해 상당히 뒤쳐져 있음

◇ 탐사획득자료 처리 및 시료의 분석기술은 선진국 기술수준에 근접한 것으로 평가됨. 특히, 최근 미세시료의 동위원소 분석 및 연대측정이 가능한 슈림프(SHRIMP) 장비가 도입됨으로서, 국내의 지화학 분석의 기술수준을 한 단계 끌어올림

2.4. 선진국 수준과의 비교

◇ 1970년대 후반 동태평양해령과 갈라파고스해령에서 유인잠수정인 앨빈(Alvin)을 이용한 해저열수분출의 발견 이후 첨단 유/무인잠수정 및 탐사시스템이 도입되어온 선진국과 아직 심해에서의 독자적 잠수정 탐사를 수행한 경험이 없는 우리나라의 심해 근접해저면 탐사기술의 격차는 상당히 존재함

◇ 하지만, 우리나라 역시 지난 20년간의 심해저 탐사 수행을 바탕으로 조사선 및 광역탐사 기술은 선진국 수준에 근접해있는 것으로 평가할 수 있으며, 최근 쇄빙연구선이 새로 건조됨에 따라 해당 기술수준격차는 더욱 줄어든 것으로 판단됨

◇ 해저열수분출 연구는 국제공동연구의 형태로 진행되는 사례가 많으며, 특히 우리나라가 갖추지 못한 근접해저면 탐사 장비의 경우 선진연구기관과의 공동연구 추진을 통해 활용할 수 있을 것으로 예상함

◇ 해석 및 분석수준은 선진국수준에 접근한 것으로 평가됨(2.3 참조)

3. 연구개발 목표

□ 활동성 및 비활동성 열수분출 지역 탐지 기술/장비 개발
□ 활동성 및 비활동성 분출구 주변의 지질/화학/생물 특성의 변화 파악
□ 해저열수활동이 생성되는 지구조환경 특성을 이해
□ 열수작용의 조성 및 규모에 영향을 미치는 요인을 이해

3.1. 최종목표

□ 해저열수분출지역의 지역적 다양성을 파악하고 생성 및 진화시기에 따른 분출구 및 주변 환경 특성 변화를 이해함으로서 활동성 분출지역에 한정되어 있는 해저열수분출 시스템에 대한 인식의 폭을 비활동성 지역으로 확대함

□ 과거에 형성된 비활동성 및 소멸성 열수분출지역에 대한 탐지기술과 장비를 확립하고 이들 지역에서의 금속광체의 보존 여부, 보존지역 규모 등 잠재 자원가치를 평가함

3.2. 단계별 연구 목표

□ **제 1단계 (2010년-2012년): 활동성 및 비활동성 열수분출지역 탐사기술 확립**

열수활동 지역 평가를 통해 활동성 및 비활동성 열수분출지역이 공존하는 탐사지역을 선정함. 선정된 탐사지역을 대상으로 광역플룸 조사 및 근접 해저면 지형/영상자료 획득을 이용한 활동성 열수분출지역을 판별하고, 지자기 조사기법을 통해 열수분출이 멈춘 비활동성 분출지 및 퇴적물/용암으로 피복된 소멸성 열수분출지역을 파악함. 특히, 자율형 수중탐사체(AUV)를 이용한 원격탐사 기법을 외국연구기관과 공동으로 탐사현장에 적용함

□ **제 2단계 (2013년-2015년): 활동성/비활동성 열수분출지역의 지질/화학/생물 특성 파악**

1단계를 통해 확인된 활동성/비활동성 열수분출지역을 대상으로 연대측정을 통해 열수활동 시기를 판별하고 진화단계를 파악함. 열수분출지역의 기반암/지구조 특성을 이해하고 이들 지질특성에 따른 분출구 주변 생물 특성과의 상관성을 이해함. 또한 비활동성 열수분출지역을 대상으로 열수분출구의 해수에 의한 산화 및 변질과 그에 따른 주변 생태 특성 변화를 해석. AUV를 이용한 원격탐사 기법 및 장비 개발

□ **제 3단계 (2016년-2019년): 해저열수분출지역의 시공간적 다양성을 이해하고, 활동성/비활동성 분출지역의 규모 해석**

1단계와 2단계에서 도출된 결과를 바탕으로 활동성 및 비활동성 열수분출지역의 규모를 파악하고 생성규모에 영향을 주는 요인을 해석함. 또한 비활동성 열수분출지역의 산출 빈도와 범위를 파악함. 열수분출지역의 진화에 따른 분출지역의 지질/화학 특성변화가 주변 생태계에 미치는 영향 파악하고 이를 통해 열수분출지역의 생성/소멸 주기성을 해석. 지형/지질, 열수추적자, 지자기 등 활동성/비활동성 열수분출지를 탐지하기 위한 독자적 원격탐사시스템 구축

4. 연구내용 및 범위

4.1. 단계별 수행 연구 개발 과제

단 계	연구 개발 과제
제 1단계 (2010년-2012년) 활동성 및 비활동성 열수분출지역 탐사기술 도입	▶ 열수활동 지역 평가를 통한 활동성/비활동성 열수분출지역이 공존하는 탐사 후보지역 선정 ▶ 광역플룸 조사 및 근접해저면 지형/영상자료 획득을 통한 활동성 열수분출지역 추적기법 수립 ▶ 열수분출이 멈춤 비활동성 분출지 및 퇴적물/용암류로 피복된 소멸성 열수분출지의 검출을 위한 지자기 조사기법 개발 ▶ 자율형수중탐사체 (AUV)를 활용한 원격탐사기법 적용
제 2단계 (2013년-2015년) 활동성/비활동성 열수분출지역에 대한 지질/화학/생물 특성 파악	▶ 활동성/비활동성 열수분출지역의 연대측정 ▶ 열수분출지역 기반암/지구조 특성 및 생물군집 파악 ▶ 비활동성지역의 열수분출구의 변질 및 주변 생태 특성 변화 해석 ▶ AUV를 이용한 원격탐사기법 및 장비 개발
제 3단계 (2016년-2019년) 해저열수분출지역의 시공간적 다양성을 이해하고, 활동성/비활동성 분출지역의 규모 해석	▶ 비활동성 열수분출지역의 산출 빈도 및 범위 파악 ▶ 활동성/비활동성 열수분출지역의 규모해석 및 영향요인 파악 ▶ 열수분출지역의 진화에 따른 분출구의 지질/화학 특성변화가 주변 생태계에 미치는 영향 파악 ▶ 열수분출지역의 생성/소멸 주기성 해석 ▶ 활동성/비활동성 열수분출지역 탐지를 위한 독자적 원격탐사기술 구축

4.2. 연구대상기술의 개발 가능성

◇ 활동성 및 비활동성 열수분출지역 원격탐사기술 구축

○ 현재 활동성 열수플룸의 추적기술은 구축되어 있으며, DTSSS를 활용한 근접해저면 지형/지질 특성과 연동한 열수분출지 추적은 현재의 연구인프라로 가능함

○ 비활동성 열수분출지역 탐사기술은 심해 지자기 탐사기법을 이용해야하며, 현재 일부 탐사경험이 수립되어 있음. 하지만, 탐사기법상 AUV를 활용한 원격탐사시스템을 도입하는 것이 유리하며, 이를 위해 WHOI의 ABE 등 AUV 활용을 위한 공동연구 수행을 통해 연구 가능함

○ 현장조사팀과 장비개발팀의 융합을 통해 현장 적용 가능한 원격탐사기술의 독자적 구축이 가능함

◇ 활동성/비활동성 열수분출지역에 대한 지질/화학/생물 특성 파악

○ 열수분출지역의 연대측적은 현재 국내에 도입되어 있는 동위원소분석 시스템을 활용하여 수행가능함

○ 열수분출지역의 시료채취를 위한 근접해저면 조사는 ROV의 활용을 통해 가능하며, 이를 위해 실해역 조사 기능을 갖춘 ROV 탐사 수행이 요구됨. 국내에서는 아직 ROV를 활용한 열수지역 탐사 경험이 부족하며, 외국연구기관과의 공동연구 수행이 필요함

○ 열수분출지역에서 채취된 다양한 시료의 분석 및 해석은 해양연구원 내 구축된 인력풀 및 국내 대학과의 공동연구 수행을 통해 달성 가능

◇ 해저열수분출지역의 시공간적 다양성을 이해하고, 활동성/비활동성 분출지역의 규모 해석

○ 열수분출지역의 분포범위, 규모해석, 주기성 해석 등은 해당 1-2단계 사업 수행 결과의 종합해석을 통해 달성 가능함

○ 현재 InterRidge의 “Seafloor Mineralization” Working Group에서는 비활동성 열수분출지역을 연구하기 위한 전문가 모임이 구성되어 있으며, 이를 통한 공동연구 수행이 가능함

4.3. 기술개발 및 시장점유 가능성

해당사항 없음

5. 연구개발 추진전략 및 체계

5.1. 기본방안

◇ **현장 조사와 탐사장비 개발의 동시 추진**

- 국내에 갖추어지지 않은 장비 및 기술의 적용은 선진연구기관과의 공동연구를 통해 수행한 이후, 독자적 기술개발 및 탐사 수행을 추진
- 초기단계부터 해양조사팀과 기술개발팀이 함께 결집하여 전시용이 아닌 최종사용자가 실해역 연구에 활용될 수 있는 탐사기술/장비 개발

◇ **국내 산·학·연의 연구역량을 결집**

- 대학, 연구기관, 관련 산업체 등 핵심연구 인프라를 포괄하는 통합 연구체제 구축
- 현장조사, 탐사기술개발, 첨단 분석 등의 전문 역량의 유기적 관계 구축 및 통합 자료 해석

◇ **선진연구기관 및 국제연구그룹과의 공동연구 수행**

- InterRidge의 “Seafloor Mineralization" Working Group*과의 공동연구 수행을 통해 연구 초기단계에서 노출되는 장비 및 기술 격차를 극복하고 독자적 연구시스템 기반 구축

* InterRidge "Seafloor Mineralization" Working Group 구성

이름	국적	소속	전문분야
Maurice Tivey	미국	WHOI	지구물리/지구조
Georgy Cherkashov	러시아	VNIIOkeangeologia	광물/지화학
Yves Frouquet	프랑스	IFREMER	광물/지화학
Mark Hannington	캐나다	Univ. of Ottawa	광상학
K.A. Kamesh Raju	인도	NIO	지구물리/지구조
Yashhiro Kato	일본	JAMSTEC	지화학
Jonguk Kim	한국	KORDI	광물/지화학
Lisa Levin	미국	SIO	저서생물
Rachel Mills	영국	NOC	지화학
Xuefa Shi	중국	FIO	광물/지화학
Ingunn Thorseth	노르웨이	Univ. of Bergen	저서생물
Cindy Von Dover	미국	Duke Univ.	저서생물
Fernando Barriga	포르투갈	Univ. of Lisbon	광상학

5.2. 추진전략

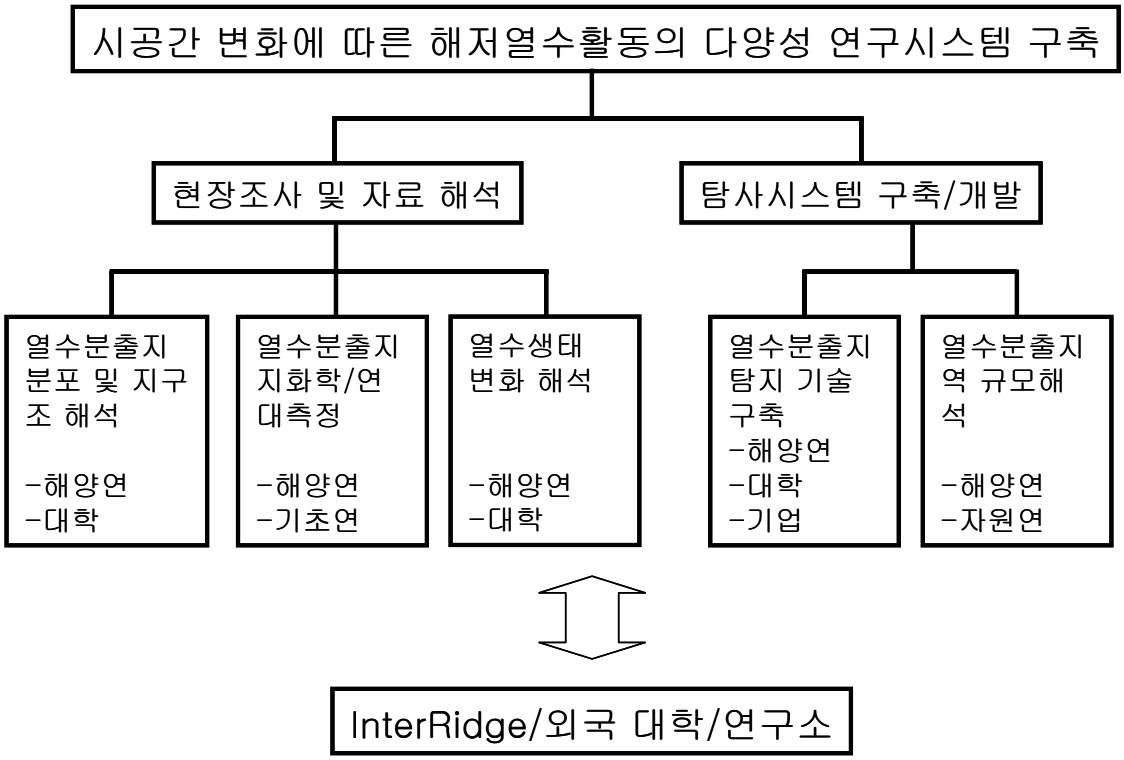

가. 세부추진전략

- 사업 초기단계에서 InterRidge, 외국대학 및 연구소와의 공동연구 추진을 통해 최고수준의 현장자료 획득을 담보하고 탐사시스템 구축에 필요한 기술수준 확보. 특히, 해저열수연구 관련 실해역 탐사에 연구원의 상호교류를 적극적으로 추진함
- 국내 참여기관 (연구소, 대학, 산업체)의 공동연구의 경우 사업단계에 따라 참여도의 차별화를 부여하여 단계별 목표 달성을 위한 분야별 집중화 수행
- 실제 현장에서 활용 가능한 활동성/비활동성 열수탐사 시스템 구축/개발을 위해 현장 조사 연구팀과 탐사시스템 개발팀의 정기적 아이디어 공유체계를 운영하고 기술개발팀을 현장조사 참여를 적극 유도

나. 단계별 추진전략

추진단계	기본방안	추진전략
제 1단계 2010-2012	활동성 및 비활동성 열수분출지역 탐사기술 도입	▪ 활동성/비활동성 열수분출지역이 근접한 실해역 탐사지역의 선정 ▪ 활동성 열수탐지 기술시스템 확보 ▪ 비활동성 열수분출지역 탐지를 위한 공동연구시스템 구축 ▪ 원격탐사체를 이용한 열수분출지역 탐지를 위한 공동탐사 수행
제 2단계 2013-2015	활동성/비활동성 열수분출지역에 대한 지질/화학/생물 특성 파악	▪ 열수분출지역의 지질/생물 시료 채취기술 확보 ▪ 열수시스템의 연대측정기법 개발 ▪ 활동성 및 비활동성 열수분출지역의 시기에 따른 지화학/생물 변화 파악 ▪ 열수분출 탐지를 위한 원격탐사체 도입
제 3단계 2016-2018	해저열수분출지역 의 시공간적 다양성을 이해하고, 활동성/비활동성 분출지역의 규모 해석	▪ 비활동성 열수분출지역의 산출 빈도 및 범위 파악 ▪ 열수분출지역의 진화에 따른 분출구의 지질/화학 특성변화가 주변 생태계에 미치는 영향 파악 ▪ 열수분출지역의 생성/소멸 주기성 해석 ▪ 활동성/비활동성 열수분출지역 탐지를 위한 독자적 원격탐사기술 구축

5.3. 연구개발 추진일정

분류	핵심기술 연구내용	1단계			2단계			3단계			비고
		10	11	12	13	14	15	16	17	18	
	▪ 열수활동 지역 평가를 통한 활동성/비활동성 열수분출지역이 공존하는 탐사 후보지역 선정 ▪ 광역플룸 조사 및 근접해저면 지형/영상자료 획득을 통한 활동성 열수분출지역 추적기법 수립 ▪ 열수분출이 멈춤 비활동성 분출지 및 퇴적물/용암류로 피복된 소멸성 열수분출지의 검출을 위한 지자기 조사기법 개발 ▪ 자율형수중탐사체 (AUV)를 활용한 원격탐사기법 적용										
	▪ 활동성/비활동성 열수분출지역의 연대측정 ▪ 열수분출지역 기반암/지구조 특성 및 생물군집 파악 ▪ 비활동성지역의 열수분출구의 변질 및 주변 생태 특성 변화 해석 ▪ AUV를 이용한 원격탐사기법 및 장비 개발										
	▪ 비활동성 열수분출지역의 산출 빈도 및 범위 파악 ▪ 활동성/비활동성 열수분출지역의 규모해석 및 영향요인 파악 ▪ 열수분출지역의 진화에 따른 분출구의 지질/화학 특성변화가 주변 생태계에 미치는 영향 파악 ▪ 열수분출지역의 생성/소멸 주기성 해석 ▪ 활동성/비활동성 열수분출지역 탐지를 위한 독자적 원격탐사기술 구축										

6. 기대성과 및 활용방안

6.1. 기대성과

기 대 성 과

▶ 접근이 제한된 극한지역에 분포하는 해저열수 분출지역을 탐지하기 위한 원격탐사 시스템 개발은 현재 활용되고 있는 최고수준의 해양연구 탐사기술이 집약되어야 하며, 이를 통해 국내의 해양연구 탐사 수준을 선진국 수준으로 진일보할 수 있음

▶ 과거의 열수활동에 의해 생성된 비활동성/소멸성 열수분출지역에 대한 탐사기술을 개발하고 물성변화에 따른 잠재 자원가치를 평가함으로서 해저광물자원 개발대상을 확대시킬 수 있음

▶ 열수분출의 진화에 따른 구성요인 특성변화를 파악함으로서 열수생태계라는 중요한 생명환경의 보존을 담보할 수 있는 기반을 구축함

6.2. 활용방안

활 용 방 안

▶ 열수진화에 따른 열수분출지역의 지질/생물학적 변화를 파악함으로서 해저열수광상개발에 대한 광업규칙 및 지침 제정에 주도적으로 대처하고 우리의 국익이 극대화될 수 있는 관련 법/규칙 제정 유도 방향을 제시하는데 활용될 수 있음

▶ 열수분출지역 탐지를 위한 원격탐사 시스템은 다양한 목적의 해저면 탐사에 널리 이용될 수 있음. 특히, 해저자원 개발을 위한 탐사에 매우 유용하게 활용될 것임

▶ 21세기 해양시대를 주도할 해양개발기술의 획기적 발전을 이룩하고 새로운 해양산업을 창출하는 등 기술파급 및 해양산업기술 발전유도

7. 결론 및 정책적 시사점

7.1. 결론

결 론

▶ 해저열수활동은 해양과 지구내부(지각, 맨틀) 사이의 물질 및 에너지 교환의 장으로 물리/화학/지질/생물 등 지구과학의 전분야가 융합된 거대과학의 연구토대를 제공하지만 국내의 관련 연구는 열수활동의 결과물인 해저열수광상의 자원 개발에 치중되어 새로운 연구의 패러다임이 필요함

▶ 현재 알려진 활동성 열수분출구의 연대는 수십 년에서 수만 년으로 다양하며, 열수분출의 생성주기 또한 생성지역에 따라 차이가 큰 것으로 파악됨. 하지만, 열수분출의 중지와 소멸에 따른 분출구의 변화(변질작용, 생물군 변화 등)는 아직 잘 알려져 있지 않음

▶ 해저열수활동이 화산활동에 수반됨을 감안할 때 과거의 열수작용에 의해 생성된 열수분출지역(extinct vent)은 활동성 열수지역에 비해 더 많이 분포하고 있을 것으로 예측되나 그 탐지기술은 아직 초기단계에 머물러 있으며, 원격탐사 기술이 주로 사용될 수 있을 것으로 예측되고 있음

▶ 시공간에 따른 해저열수활동 다양성 연구는 주로 활동성 지역에 한정되어 있는 해저열수분출 연구의 공간을 비활동성 지역으로 확대할 수 있는 토대를 마련하며, 이는 열수분출 및 그 구성요소의 진화에 대한 이해의 폭을 넓히는 한편, 열수생태계라는 중요한 환경에 대한 피해를 최소화하면서 해저열수광상을 개발에도 활용될 것임

7.2. 정책적 시사점

정책적 시사점

▶ 이 연구를 통해 극한환경에 분포하는 해저열수 분출지역에 대한 원격탐사체 탐지기술을 확보함으로서 우리나라의 해양 연구개발의 수준을 한 단계 끌어올리는 동시에 보다 향상된 연구 자료를 토대로 국가적 현안인 해양영토관리, 해양환경보전 등의 정책수립을 지원함

▶ 해저열수 분출지역의 진화 연구를 통해 과거열수활동에 의한 열수분출지역의 보존여부 및 잠재 자원가치를 평가함으로서 해저광물자원 개발의 영역을 확장시킬 수 있음

8. 소요예산

□ 총 연구비 : 180억(9 년간)

(단위 : 억원)

분 야	1단계			2단계			3단계			합 계
	'10	'11	'12	'13	'14	'15	'16	'17	'18	
열수분출지역 분포 및 지구조해석	3	3	3	4	5	5	3	3	3	32
열수분출지역 지화학 및 연대측정	3	3	3	4	5	5	3	3	3	32
열수생태변화 해석	1	2	2	2	5	5	4	4	4	29
열수분출지 탐지기술 구축	1.5	4	4	5	10	10	3	3	3	43.5
열수분출지역 규모 해석	1.5	3	3	5	5	5	7	7	7	43.5
계	10	15	15	20	30	30	20	20	20	180

Chapter II. 연구 논문 성과

1) 김종욱, 손승규, 손주원, 김경홍, 심원준, 김창환, 이경용 (2009) Venting sites along the Fonualei and Northeast Lau Spreading Centers and evidence of hydrothermal activity at an off-axis caldera in the northeastern Lau Basin. Geochemical Journal, 43: 1-13.

Geochemical Journal, Vol. 43, pp. 1 to 13, 2009

Venting sites along the Fonualei and Northeast Lau Spreading Centers and evidence of hydrothermal activity at an off-axis caldera in the northeastern Lau Basin

JONGUK KIM,[1]* SEUNG-KYU SON,[1] JU-WON SON,[1] KYEONG-HONG KIM,[1] WON JOON SHIM,[2] CHANG HWAN KIM[3] and KYEONG-YONG LEE[1]

[1]Deep-sea & Marine Georesources Research Department, Korea Ocean Research & Development Institute, Ansan P.O. Box 29, Seoul 425-600, Korea
[2]South Sea Institute, Korea Ocean Research & Development Institute, 391 Jangbuk-ri, Jangmok-myon, Geoje-shi 656-830, Korea
[3]Dokdo Research Center, Korea Ocean Research & Development Institute, Ansan P.O. Box 29, Seoul 425-600, Korea

(*Received June 28, 2007; Accepted July 14, 2008*)

The regional distribution of hydrothermal vent activity in the northeastern (NE) Lau Basin was recently reported by the Ridge 2000 program; however, active venting sources have yet to be located. Here, we report geological and hydrological evidence that indicates the presence of three active hydrothermal venting sources in the NE Lau Basin: the Fonualei Rift and Spreading Center (FRSC), the Northeast Lau Spreading Center (NELSC), and an off-axis caldera (MTJ-1). These examples of hydrothermal activity were recognized by the appearance of hydrothermal plume signals in the water column, including anomalies in light-transmission, methane, adenosine 5′-triphosphate (ATP), and trace metal concentrations (TDMn and TDFe). Three active venting sources were identified by the observation of possible buoyant plumes during conductivity-temperature-depth (CTD) tow-yo surveys and by the recovery of hydrothermal precipitates (chimneys and altered rocks). The strongest light-transmission anomaly, an order of magnitude greater than those at other sites, was observed at the central cone of the MTJ-1 caldera. The recovery of eruption debris at a central volcanic cone, including molten sulfur, volcanic ash, and lapilli, indicates an active volcanic eruption and hydrothermal venting at the MTJ-1 caldera. Our results suggest extensive and various hydrothermal activity in the NE Lau Basin, thereby providing valuable insight into hydrothermal and volcanic processes in back-arc environments.

Keywords: hydrothermal venting, back-arc spreading, off-axis caldera, NE Lau Basin, SW Pacific

INTRODUCTION

The Lau Basin is a back-arc basin behind the Tonga Trench that separates the remnant Lau ridge volcanic arc from the active Tonga Arc (Hawkins, 1995). The Lau Basin has a complex morphology formed by subduction-related histories of extension and spreading within the basin. At present, six active spreading centers, including the Central Lau Spreading Center (CLSC), Eastern Lau Spreading Center (ELSC), Fonualei Rift and Spreading Center (FRSC), Northwest Lau Spreading Center (NLSC), Fotuna Spreading Center (FSC), and Northwest Lau Spreading Center (NWLSC), have been postulated to exist within the Lau Basin (Zellmer and Taylor, 2001). Several hydrothermal venting sites have been reported along the axes of the CLSC, ELSC, FRSC, and along the Northeast Lau Spreading Center (NELSC) (e.g., Fouquet *et al*., 1991; Herzig *et al*., 1993; Baker *et al*., 2006; German *et al*., 2006; Martinez *et al*., 2006).

The first hydrothermal survey of the NE Lau Basin was conducted during KM0417 cruise of the R/V *Kilo Moana* in 2004 (German *et al*., 2006). Hydrothermal plume signals were identified in four areas, three along the FRSC and one on the NELSC, by a series of point measurements made using a plume detector (Miniature Autonomous Plume Recorders, MAPRs) mounted on a rock core and dredge. These results imply that abundant hydrothermal venting is currently occurring along the back-arc spreading centers in the NE Lau Basin, possibly explaining the regional ^{3}He anomaly in the Tonga–Fiji region of the South Pacific Ocean (Lupton *et al*., 2004). However, active venting sites have not yet been located by point measurements, although German *et al*. (2006) suggested that some of their stations were within several kilometers of active venting sources.

Annual hydrothermal expeditions aboard the R/V

*Corresponding author (e-mail: jukim@kordi.re.kr)

Onnuri have been undertaken by the Korea Deep Ocean Study (KODOS) program in the NE Lau Basin since 2004. Regional hydrothermal plume signals along the FRSC were detected for the first time using several vertical conductivity-temperature-depth (CTD) castings during the KODOS H04 cruise in December 2004 (Kim *et al*., 2006b). A more detailed geophysical survey and sampling were performed at the FRSC and MTJ-1 caldera during the KODOS H05 cruise in December 2005, when an extensive hydrothermal plume signature was discovered at the MTJ-1 caldera (Kim *et al*., 2006b). During KODOS H06 cruise in December 2006, CTD tow-yo surveys were performed over the potential hydrothermal venting areas indicated by the two previous cruises to investigate the precise distribution of the hydrothermal plume. In this paper, we present the spatial distribution of the hydrothermal plume signal (light-transmission anomaly) detected using CTD tow-yo and the occurrence of a hydrothermal chimney, which indicate the locations of active venting sites along the FRSC and NELSC. We also provide evidence of a further hydrothermal venting site at an active off-axis caldera near the NELSC.

Study Area and Geological Setting

The study area included two sections of back-arc spreading centers, the FRSC and NELSC, and one off-axis caldera (designated "MTJ-1") in the NE Lau Basin (Fig. 1). The FRSC extends south of the Mangatolu Triple Junction (MTJ) and represents the plate boundary between the Tonga Plate and the Niuafo'ou microplate (Zellmer and Taylor, 2001). The FRSC is composed of numerous small, overlapping rifts and spreading segments; seismic and magnetic data suggest that its spreading rate increases from 47 mm/yr at its southernmost extent to 85 mm/yr at its northernmost tip (Zellmer and Talyor, 2001). The distance between the spreading axis of the FRSC and the adjacent Tonga Arc varies from ~25 km at 18°S to ~75 km at 16°S (Fig. 1). The variation of spreading rate along the FRSC is directly analogous to the variations observed along the Valu Fa Ridge and ELSC in the southern Lau Basin, although in these cases the variations in spreading rate are more gradual and occur along almost twice the length of spreading axis as that along the FRSC (German *et al*., 2006).

The NELSC lies northeast of the FRSC and parallel to the NE branch of the MTJ (Fig. 1). The proximity of the NELSC to the Samoan hotspot suggests that this area is influenced by the hotspot plume, which possibly affects both the volcanic and hydrothermal activities of the NELSC, as on the East Scotia Rise and in the North Fiji Basin (Kim *et al*., 2006a; Baker *et al*., 2005). After consideration of other overlapping spreading centers, German *et al*. (2006) proposed that the spreading rate along the NELSC is similar to that of the NE branch of the MTJ (i.e., ~94 mm/yr), although its tectonic setting is poorly constrained.

The MTJ-1 caldera is located ~45 km east of the NELSC and ~90 km west of the northern Tofua Arc (Fig. 1). The caldera is composed of a circular caldera wall of ~10 km in diameter and a central volcanic cone. The summit elevation of the central cone lies at about 1300 m water depth. A second, less prominent cone (~1500 m) occurs to the southeast of the first cone (Fig. 1). Bloomer and Wright (1996) reported that the caldera is composed of dacite lavas, which may have been derived from both the adjacent Tonga Arc and the back-arc spreading center. Arculus (2004) reported strong hydrothermal plumes near the summit of the central cone, and recovered sulfide-rich material and small spheroids of native sulfur by dredging the northwest flank of the cone; however, no intensive hydrothermal investigations have been reported at MTJ-1.

Methods

Most of the sampling and survey data presented in this study were obtained during the KODOS H06 cruise of the R/V *Onnuri* in December 2006 (Kim *et al*., 2007); however, some data were collected from two previous cruises that surveyed hydrothermal activity in the NE Lau Basin (Table 1). We used CTD tow-yo at the FRSC, NELSC, and MTJ-1 to investigate the precise distribution of the hydrothermal plume (Fig. 1). The principal method employed in the hydrothermal investigation involved the measurement of light transmission, which decreases with particle abundance, which itself increases when metals and sulfur are vented and precipitate when mixed with seawater. For CTD tow-yo, we used high-precision CTD (SeaBird, 911 plus) with a light transmissometer (Otronix, WetLabs C-star). Two CTD tow-yo surveys were performed for each targeted area to determine the distribution of the plume. The second tow-yo line was set up perpendicular to the first line at the point of the maximum light-transmission anomaly (Fig. 1). Seawater was sampled using vertical CTD casting to measure methane, adenosine 5′-triphosphate (ATP), and trace metals. The CTD system (SeaBird, 911 plus) was equipped with a light transmissometer (Otronix, WetLabs C-star) and a 24-position rosette attached to 10 L Niskin bottles. Rocks were sampled using a chain-bag dredge at the target sites, which were selected as possible buoyant plumes identified during the CTD tow-yo surveys. Hydrothermal chimneys and/or hydrothermally altered rocks were sampled from four sites in the study area (arrows in Fig. 1).

The methane in water samples was analyzed according to the method suggested by Ohta *et al*. (1999), with a

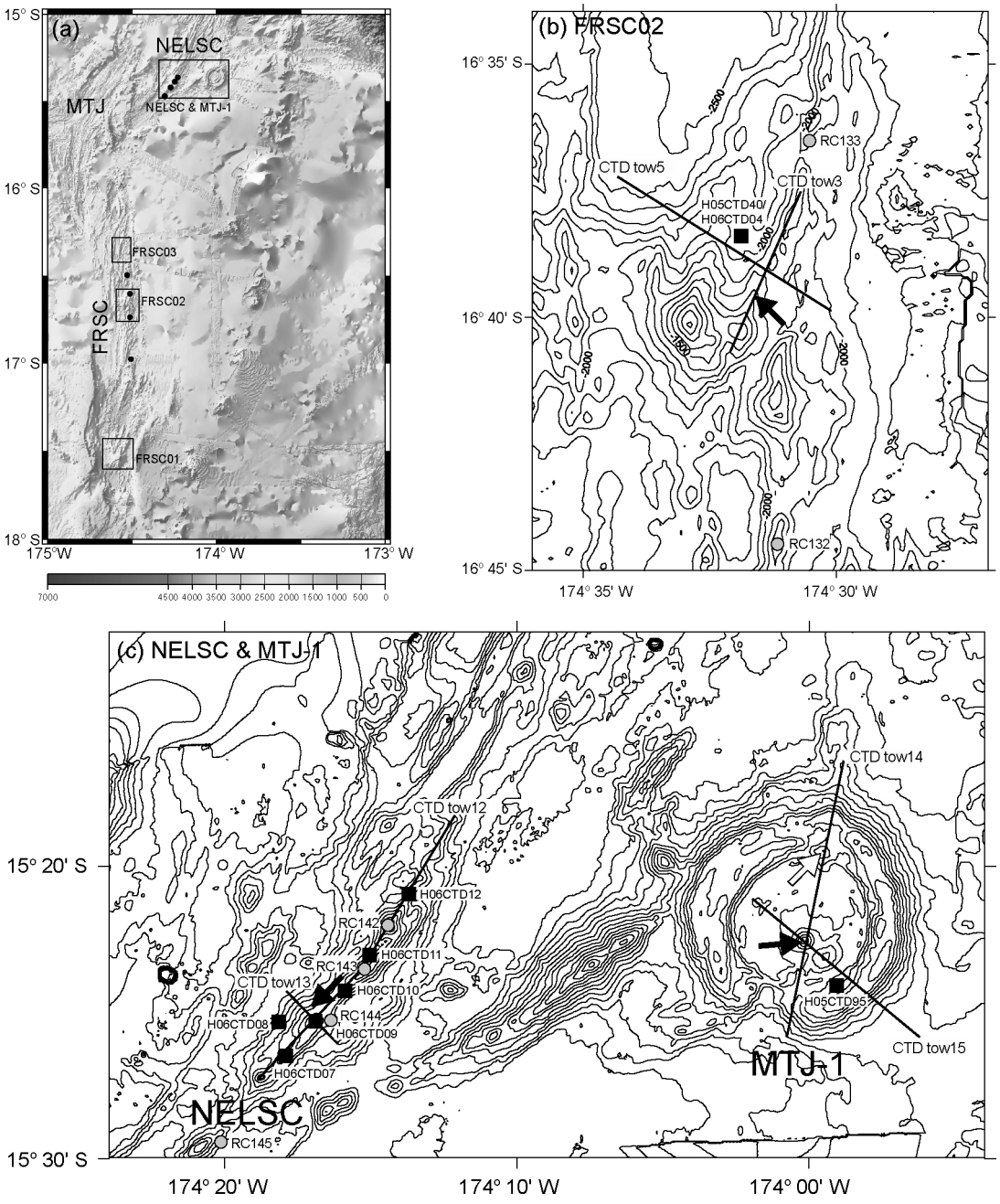

Fig. 1. Bathymetric map of the NE Lau Basin (modified from Martinez and Taylor, 2006), indicating our principal survey area (a). Black dots indicate the locations of the plume signals reported by German et al. (2006). FRSC, Fonualei Rift and Spreading Center; MTJ, Mangatolou Triple Junction; NELSC, Northeast Lau Spreading Center. Detailed bathymetric maps of the FRSC02 (b) and NELSC and MTJ-1 sites (c). Locations of their active hydrothermal vent sites are indicated by black arrows. The white arrow at MTJ-1 indicates an extinct hydrothermal site. The CTD tow-yo path and vertical CTD casting are presented as lines and black squares, respectively. Gray circles are the locations of the plume signals observed by German et al. (2006).

minor modification. A water sample collected with a Niskin bottle was siphoned into a 100 mL serum bottle with a butyl-rubber stopper and an aluminum sealer. Gas was separated from the water using the headspace method in the following manner. To create the headspace, a 10 or 20 mL portion of the water sample in the capped serum bottle was replaced with synthetic zero air (99.9999%) purchased from Wintree Corp. The bottle was then vigor-

Table 1. Locations and dates of survey stations

Station	Date and Time (GMT)	Latitude S	Longitude W	Depth m
FRSC				
H05CTD40	2005.12.22. 15:02	16°38.51′	174°32.04′	2032
CTD tow3	2006.12.22. 22:26	16°40.49′	174°32.07′	1521
		16°36.87′	174°30.41′	2065
CTD tow5	2006.12.23. 07:00	16°37.87′	174°33.27′	2199
		16°40.45′	174°30.01′	1888
H06DG04	2006.12.23. 19:18	16°39.27′	174°31.53′	1724
		16°39.59′	174°31.63′	1643
H06CTD04	2006.12.24. 00:45	16°38.53′	174°32.08′	1980
NELSC				
CTD tow12	2006.12.26. 00:21	15°26.48′	174°17.86′	1787
		15°18.86′	174°12.85′	2005
CTD tow13	2006.12.26.12:25	15°23.47′	174°17.62′	2439
		15°26.62′	174°15.74′	2373
H06CTD07	2006.12.26. 19:09	15°26.24′	174°17.55′	1852
H06CTD08	2006.12.27. 01:35	15°25.40′	174°17.62′	1819
H06DG12	2006.12.27. 05:51	15°25.17′	174°17.06′	1530
		15°25.70′	174°17.02′	1756
H06CTD09	2006.12.27. 08:18	15°25.32′	174°17.04′	1549
H06CTD10	2006.12.27. 10:15	15°24.44′	174°16.04′	1816
H06CTD11	2006.12.27. 22:09	15°23.28′	174°15.03′	1640
H06CTD12	2006.12.28. 00:03	15°20.96′	174°13.77′	1862
MTJ-1				
H05CTD95	2005.12.30. 00:03	15°24.67′	173°59.35′	1415
CTD tow14	2006.12.28. 08:30	15°26.11′	174°01.03′	2197
		15°16.42′	173°58.78′	2126
CTD tow15	2006.12.28. 21:23	15°21.31′	174°01.98′	1773
		15°25.61′	173°56.18′	2081
H06DG18-3	2006.12.30. 05:52	15°22.27′	173°59.81′	1620
		15°22.68′	174°00.72′	1712
H06DG20	2006.12.30. 08:00	15°20.00′	173°59.72′	1699
		15°19.19′	173°59.52′	1609

ously shaken by hand for 2 min and allowed to stand for more than 5 min in the dark to complete the equilibration of the aqueous and gaseous phases. A 1 mL portion of gas was then taken from the headspace using an airtight syringe and analyzed with a gas chromatograph (GC) equipped with a semiconductor detector (GS-23, Senortec Co.). A gas sample injected into the GC was carried by the zero air (99.9999%) into the separation column (stainless steel, 2 m × 3 mm i.d.) packed with a molecular sieve 13X-S (60/80 mesh; GL Sciences Co., Tokyo, Japan). The temperature was controlled by a controller for line heaters and was maintained at 50°C and 40°C for the separation column and the detector port, respectively. A standard for CH_4 gas (0.5 and 5.0 ppm) from Wintree Corp. was used for calibration. The relative standard deviation of replicate analyses of water samples (n = 5) was 2.1% and the detection limit was 0.033 nM.

The ATP concentration in the seawater was measured onboard following the method of Bulleid (1978), with minor modifications. Microbial cells were filtered from 300 mL of sampled seawater on membrane filters (0.2 μm pore size, 25 mm diameter; Advantec MFS Inc.). These filters were placed directly into 5 mL of boiling phosphate buffer (60 mM) in test tubes and reacted for 5 min to extract microbial ATP. The extracted ATP was measured based on its reaction with luciferin-luciferase (Webster *et al*., 1984) in a luminometer (Turner Designs model 20e). The relative standard deviation of replicate analyses of two standard samples (n = 8) was less than 5% and the detection limit was 0.01 ng/L.

To measure trace metals (total dissolvable Mn and Fe, TDMn and TDFe), the sampled seawater was drawn into an acid-cleaned 1 L bottle and acidified (pH < 2) with ultrapure nitric acid to prevent the adsorption of metals. Trace metals were extracted from the acidified seawater following the method of Statham (1985) and the extracts were analyzed for trace metals using inductively coupled plasma mass spectroscopy (Thermo Elemental X-7) in the onland laboratory. The relative standard deviation of replicate analyses of standard samples (n = 5) was less than 4% and the detection limit was less than 0.9 nmol/L for both elements.

Chemical analysis was done on 13 chimney samples from the FRSC02 and NESLC and 4 hydrothermally altered rock samples from the MTJ-1 caldera (Table 2) using fusion followed by multiacid dissolution. Major and trace elements were determined via a combination analysis by ICP-AES and ICP-MS at Activation Laboratory, Canada. External precision for the analysis was less than 5%.

Results and Discussion

Hydrothermal activity at the FRSC

To characterize the spatial distribution of the hydrothermal plume signal along the FRSC, three targeted areas were selected for CTD tow-yo surveys based on the results obtained on a previous cruise; however, a significant light-transmission anomaly was observed only at the FRSC02 site by CTD tow-yo during the KODOS H06 cruise. In the other areas, indicated as the FRSC01 and FRSC03 sites in Fig. 1, no evidence of a hydrothermal plume was detected by CTD tow-yo. The results of the CTD tow-yo survey at the FRSC02 site indicated that the hydrothermal plume migrates laterally northeastward from a venting source deduced from a near-bottom light-transparency anomaly (interpreted as a possible buoyant plume) at 16°39.2′ S (Fig. 2) and also by the sampling of a hydrothermal chimney. The maximum light-

Table 2. Range and average composition of hydrothermal chimney and altered rock samples

Element	unit	FRSC02		NELSC	MTJ-1
		Sulfide-rich chimney (n = 7)	Sulfate-rich chimney (n = 2)	Sulfide-rich chimney (n = 4)	Altered rock (n = 4)
Mineralogy*		Py, Cp, Sph (Ga, Ba)	Ba, Sph (Cp, Ga)	Py, Cp (Sph, Ba)	Silicates (native S, Py, Cp)
SiO_2	%	6.13 (3.91–7.99)	2.58	<0.01–0.12	42.45 (2.63–66.06)
S	%	15.56–20<	13.85	18.38–20<	8.82 (6.45–14.7)
Fe	%	21.83 (16.3–28.8)	5.52	37.91 (31.11–44.42)	5.61 (0.99–11.05)
Cu	ppm	13068 (50–67900)	3022	35866 (32600–38700)	2374 (145–8900)
Zn	ppm	152203 (19700–208000)	201000	16567 (209–49000)	97 (52–190)
Ba	ppm	10501 (82–26610)	244100	194–119000	172 (18–251)
Ca	%	<0.01–0.15	0.13	<0.01–0.03	0.09–3.72
Al_2O_3	%	0.32–0.44	0.15	<0.01	13.83 (12.94–15.36)
Mo	ppm	36 (28–61)	18	52 (45–62)	<1
Pb	ppm	2134 (559–4000)	5860	58 (47–73)	<1
As	ppm	1512 (862–2400)	1092	203 (160–290)	141 (9–533)

**Keys: Py, pyrite; Cp, chalcopyrite; Sph, sphalerite; Ga, galena; Ba, Barite; S, sulfur.*

transmission anomaly (0.62%) was also identified by CTD tow-yo.

Hydrothermal activity at the FRSC02 site was also supported by the detection of hydrothermal plume signals, such as light transmission, CH_4, and ATP anomalies in the water column. At the vertical CTD casting station (H05 CTD40), located near the observed maximum plume anomaly (Fig. 1), light transmission showed a weak anomaly of ~0.4% in December 2005 centered between 1600 m and 1700 m water depth (Fig. 2c). Furthermore, anomalies in methane (0.95 nM at 1633 m) and ATP (8.7 ng/L at 1664 m) induced weak but clear plume signals in the water samples from the station. Although ATP is used as an indicator of active microbial biomass and is not a direct indicator of a hydrothermal plume, several studies have shown that increased microbial biomass is a common feature of plumes (Cowen *et al*., 1986; Winn *et al*., 1986). Therefore, the anomalous increases in methane and ATP in the bottom water can be explained by hydrothermal activity.

Vertical CTD casting was undertaken again at the same station (H06 CTD04) in December 2006 (Fig. 2d). Light transmission measured during the second survey had decreased slightly to ~0.1% at the same depth of 1600–1700 m. Furthermore, another light-transmission anomaly was observed at around 1200 m, with the appearance of anomalies in methane and ATP. The difference observed at the same depth between the two cruises can be attributed to advection of the plume by the local bottom current. Temporal variations in the distribution of a hydrothermal plume have been reported previously, even over periods as short as several days (e.g., Walker *et al*., 2004). Variations in the local bottom current are thought to commonly occur at the spreading axis, resulting from its complex topography. However, the occurrence of shallower plume at H06 CTD04 cannot be explained sufficiently by fluctuation of the bottom current. Some hydrothermal sites host multiple vent sources (e.g., de Ronde *et al*., 2001; Resing *et al*., 2007). The weak, shallower plume signal suggests that minor venting may also discharge on the FRSC02 site.

One large chimney sampled at the FRSC02 site showed mineral zoning typical of a black smoker, comprising a sphalerite-rich outer zone and a pyrite- and chalcopyrite-rich inner zone (Fig. 3). However, sulfate-rich chimneys with intergrowths of sphalerite and barite, which tend to precipitate at lower temperatures (150–250°C), were also collected at the FRSC02 site. Composition of the sulfide- and sulfate-rich chimneys from the FRSC02 site is shown in Table 2.

German *et al*. (2006) reported three discrete hydrothermal plume signals along the spreading axis of the

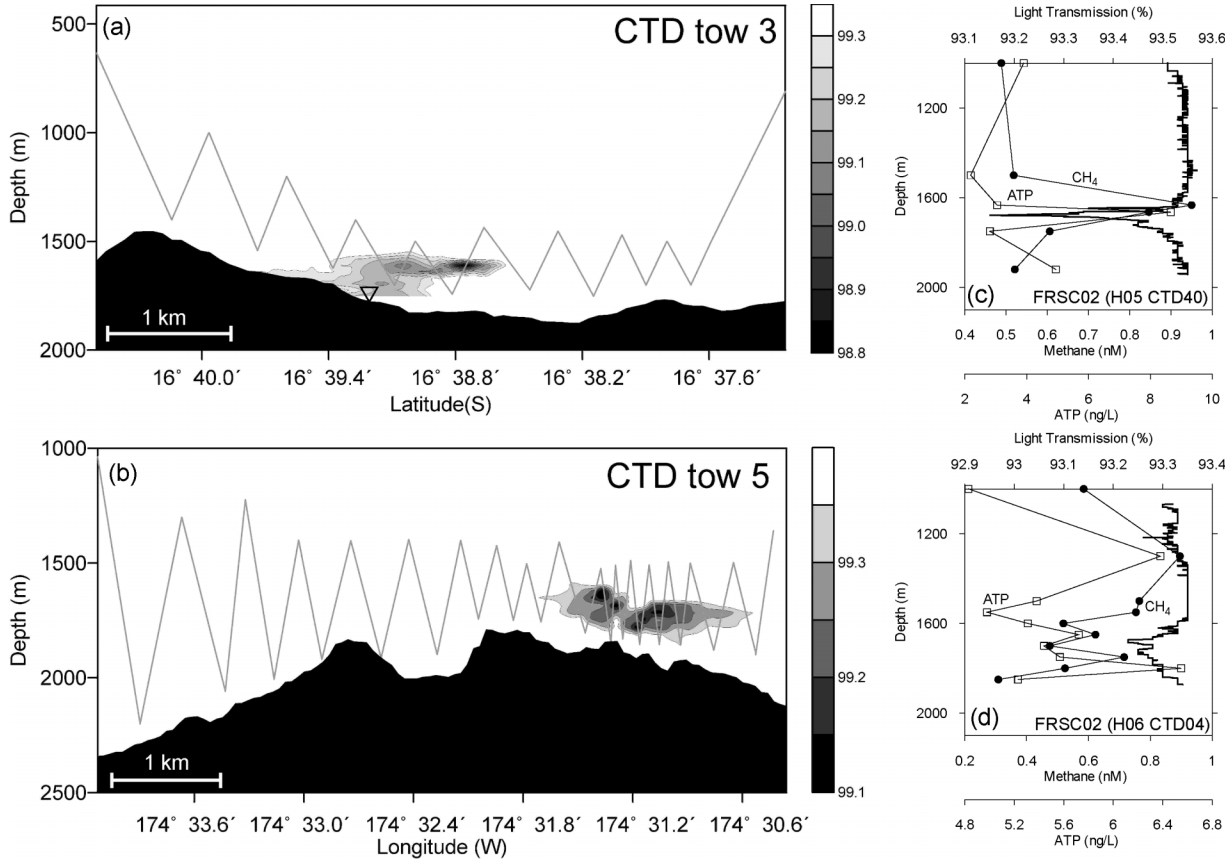

Fig. 2. Light-transmission profiles of the CTD tow3 path (a) and the CTD tow5 path (b) over the FRSC02 site. The inverted triangle in (a) indicates the location at which the hydrothermal chimney was collected. Deep-water (>1000 m) profiles of light transmission (solid line), methane (solid circles), and ATP (open squares) from vertical CTD castings H05 CTD40 (c) and H06 CTD04 (d) at the same locations during the 2005 and 2006 cruises. The locations of the paths and stations are shown in Fig. 1b.

FRSC. Station RC133, which showed the weakest plume signal of those reported by German *et al*., is located ~5 km north of the FRSC02 venting site (Fig. 1). Considering the northeastern migration of the plume, as shown in Fig. 2, the FRSC02 site is a possible venting source for the plume signal recorded at RC133; however, other hydrothermal plumes reported by German *et al*. (2006) cannot be explained by hydrothermal venting at the FRSC02 site. Thus, at least two additional hydrothermal venting sources are expected to exist along the FRSC.

Hydrothermal activity at the NELSC

Hydrothermal activity was investigated along the southern segment of the NELSC, which extends for ~18 km along a northeast trend (Fig. 1). Two volcanic summits were observed along the southern segment: a northern summit (at a water depth of 1360 m) located at 174°14.4′ W, 15°22.1′ S and a southern summit (at a water depth of 1560 m) located at 174°17.1′ W, 15°25.3′ S.

Anomalies in light transmission were recorded at various water depths along the axis of the southern segment of the NELSC (Fig. 4a). An increased anomaly, up to 1.47%, was observed between depths of 1340 m and 1500 m near the southern summit of the ridge at 15°25.3′ S. Measurements of light transmission from another tow-yo path (CTD tow-yo13), oriented perpendicular to CTD tow-yo12 at 15°25.3′ S, indicated a near-bottom light-transparency anomaly (interpreted as a possible buoyant plume) on the northwest slope of the southern summit (Fig. 4b). A hydrothermal chimney, recovered by dredging the north slope of the southern summit, was mainly composed of chalcopyrite and well-crystallized pyrite, which commonly precipitates under high-temperature conditions (>300°C). The chimney showed higher Fe and Cu concentration compared to those from the FRSC02 site (Table 2). Barite occurred as a minor mineral only in the outermost lining. The observed light-transmission anomaly and the recovery of a chimney suggest that the southern summit is an active venting site.

At the vertical CTD casting station near the southern summit (H06 CTD09), a decrease in light transmission and the maximum methane concentration at this depth

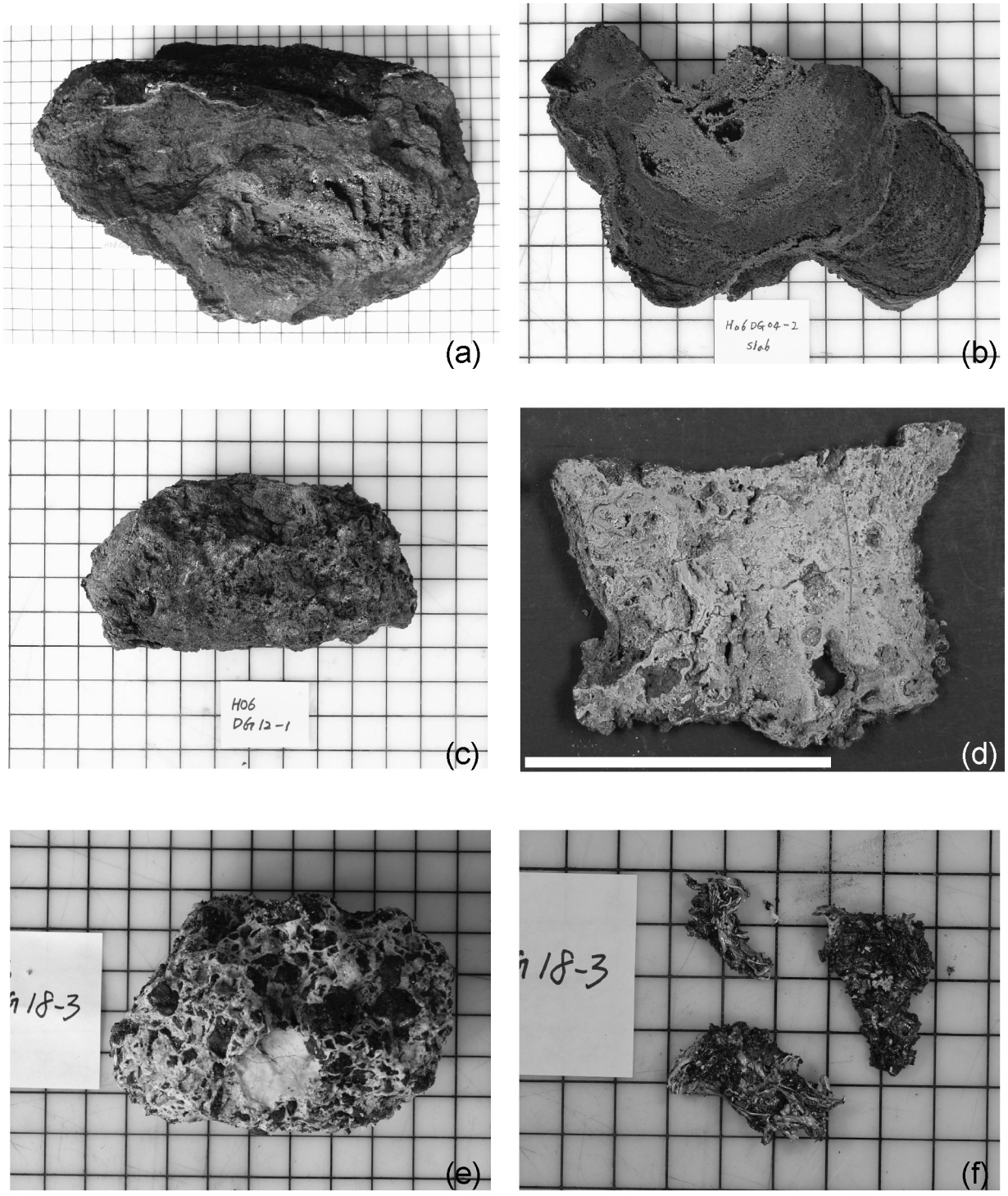

Fig. 3. (a) Photograph of a sample of hydrothermal chimney (H06 DG04-2) collected from the FRSC02 site. (b) Photograph of a section cut through the chimney (H06 DG04-2) showing the sphalerite-rich outer zone and pyrite- and chalcopyrite-rich inner zone. (c) Photograph of the hydrothermal chimney (H06 DG12-1) collected from the southern summit of the NELSC. (d) Photograph of a section cut through the chimney (H06 DG12-1). The chimney is mainly composed of chalcopyrite and well-crystallized pyrite. Scale bar is 10 cm. (e) Volcanic breccia from the central cone of the MTJ-1 caldera, composed of native sulfur, black lapilli and ash, and alunite and silica. (f) Mixture of molten sulfur and unknown black material from the MTJ-1 caldera. Grid spacing in all figures is 2 cm.

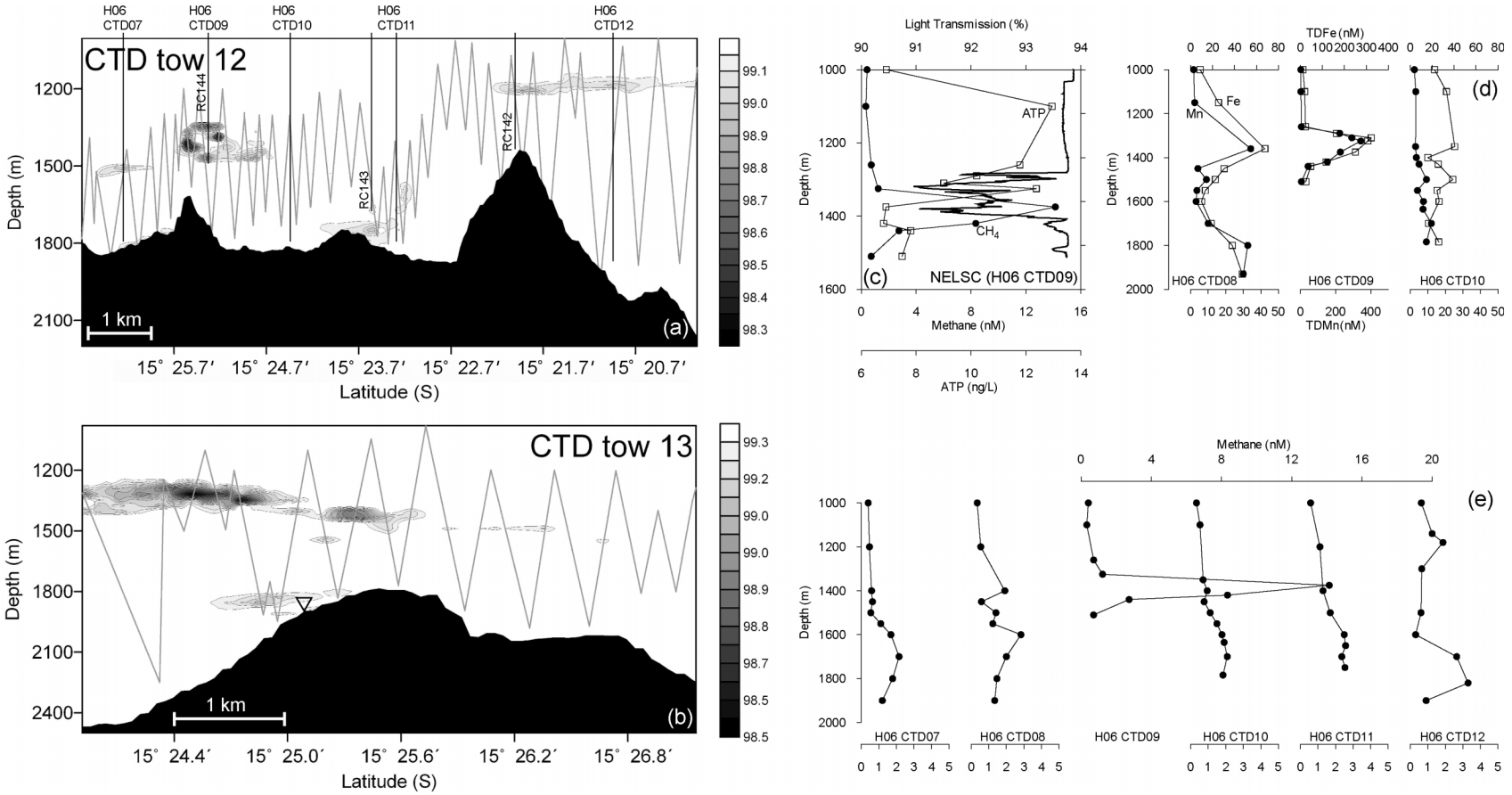

Fig. 4. Light-transmission profiles of the CTD tow12 path (a) and the CTD tow13 path (b) over the NELSC. The inverted triangle in (b) indicates the location at which the hydrothermal chimney was collected. Vertical black lines show the locations of the vertical CTD castings. Deep-water (>1000 m) profiles of light transmission (solid line), methane (solid circles), and ATP (open squares) from a vertical CTD casting (H06 CTD09) at the southern summit of the NELSC (c). Deep-water (>1000 m) profiles of trace metals (TDMn and TDFe) from three vertical CTD castings (H06 CTD08, H06 CTD09, and H06 CTD10) near the southern summit of the NELSC (d). Deep-water (>1000 m) profiles of methane along the axis of the NELSC (e). Locations of the paths and stations are shown in Fig. 1c and (a). Note that different scales for methane and metals are given for station H06 CTD09 in (d) and (e).

were estimated to be ~3.5% and ~14.1 nM, respectively. These values are approximately 9 and 15 times greater than those at the FRSC02 site (Fig. 4c). The concentrations of TDMn and TDFe were also high in the same depth interval (Fig. 4d); however, the deep-water ATP profile at H06 CTD09 did not agree with the trends of other tracers of hydrothermal plumes, although a slight peak was observed at a depth of 1325 m. Therefore, the high concentration of ATP above 1250 m at H06 CTD09 might have been related to other unknown causes rather than hydrothermal activity.

At the H06 CTD08 station, located ~1 km west of the summit, two metal-rich layers were observed at ~1400 m and ~1800 m (Fig. 4d). The reason for the enrichment of metals near the bottom is not certain, but it might be attributable to particle settling from a dispersing plume or a less buoyant (lower temperature) source near the dredge site. Other hydrothermal tracers (light-transmission, CH_4, and ATP) near the bottom at the H06 CTD08 were slightly higher than background level. The concentrations of both TDFe and TDMn showed maximum values at the H06 CTD09 station and decreased again to background levels at the H06 CTD10 station, located ~2 km northeast along the axis (Fig. 4d). Along the axis of the southern segment of the NELSC, the concentration of methane at 1400 m showed a maximum value at the H06 CTD09 station and decreased sharply to the background level at the northern stations (H06 CTD10, 11, and 12) at the same depth (Fig. 4e). At the northern stations, a methane anomaly was observed below 1500 m, with a maximum value of 3.3 nM at 1820 m at H06 CTD12; however, the methane anomaly near the bottom was not accompanied by other hydrothermal anomalies, and thus could have originated from non-hydrothermal processes.

A slight decrease in light transmission (~0.5%) was detected at a depth of ~1200 m (1100–1250 m) near the northern summit of the southern segment of the NELSC (Fig. 4a). At the H06 CTD12 station, slight anomalies in light transmission (~0.1%) and methane (up to ~1.9 nM) were observed at ~1200 m, indicating a possible non-buoyant hydrothermal plume. The venting source for this shallow plume might differ from the source of the plume at ~1400 m near the southern summit, considering its shallow depth and the northwestern dispersal of the plume at the southern summit. A possible venting source in this regard is the northern summit, where the water depth of 1360 m is sufficient for a shallow plume (Fig. 1c); however, we did not attempt bottom sampling at the northern summit and were unable to identify the location of the venting source.

German *et al*. (2006) observed hydrothermal plume signals at four stations during their study of the NELSC. They proposed that the source of the observed plume was possibly in the shallowest section of the NELSC, between stations RC143 and RC142 (i.e., the northern summit). Although the stations investigated by German *et al*. (2006) are located within our CTD tow-yo survey area (Fig. 1), the plume signals detected during our cruise (Fig. 4a) differ from the observations of German *et al*. (2006). For example, German *et al*. (2006) observed a strong plume signal between depths of 1250 m and 1500 m at RC143 (15°23.55′ S, 174°15.20′ W), which is located between the northern and southern summits. In addition, the RC144 station (15°25.32′ S, 174°17.12′ W), which was located close to the southern summit, also showed a significant plume signal near the bottom but its intensity was much lower than that of the RC143 station. On the other hand, plume signal was strongest near the southern summit at H06 CTD09 and only very weak plume signals were detected below a depth of 1700 m at H06 CTD10 and H06 CTD11, between which RC143 is located along the NELSC, in our study (Fig. 4).

The difference of plume signals between H06 CTD09 and RC144 might be spatial; i.e., German *et al*. (2006) could not observe the most intense part of a NNW drifting plume at RC144 station. However, it is obvious that the plume signal have changed significantly near the RC143 station. The plume signal at RC143 might be originated from the southern summit, which can be supported by similar depths of plume signals at H06 CTD09 and RC143. Therefore, the contrasting observations of plumes near the RC143 in these two studies could be attributable to temporal variations in the direction of bottom current.

Hydrothermal and volcanic activity in the off-axis caldera (MTJ-1)

The strongest hydrothermal plume signal was observed at a depth of about 1200 m near the central cone of the MTJ-1 caldera in the NE Lau Basin, which rises to an elevation of about 1300 m. Samples of mineralized altered rock and volcanic eruptives were also recovered by dredging the northeast flank of the cone (H06 DG18-3, Table 1). Here, the maximum anomaly in light transmission (~11.8%) was observed at 1240 m, near the central cone, using CTD tow-yo (Fig. 5). The distribution of the hydrothermal plume measured by two CTD tow-yo surveys indicates a southeastern migration of the plume from the central cone. In addition to the major plume near the central cone, another slight decrease in light transmission was observed at a lower depth (below 1500 m) near the second cone, southeast of the first (Fig. 5).

A strong light-transmission anomaly (~7.7%) was detected between depths of 1200 m and 1400 m at H05 CTD95, located southeast of the central cone; this anomaly can be divided into upper and lower plume bodies (Fig. 5c). The analyzed hydrothermal tracers (CH_4, ATP, TDFe, and TDMn) showed contrasting vertical distributions within the range of the light-transmission

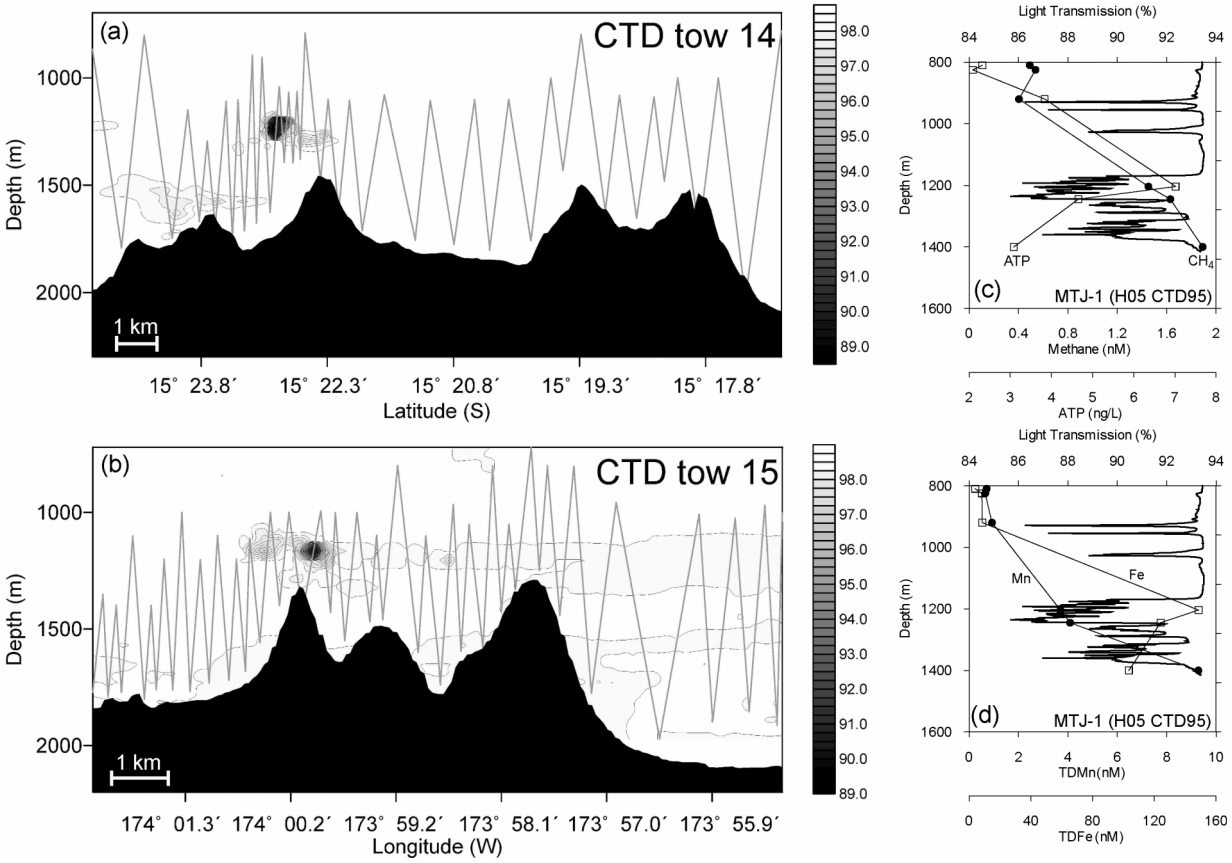

Fig. 5. Light-transmission profiles of the CTD tow14 path (a) and CTD tow15 path (b) over the MTJ-1 caldera. Deep-water (>1000 m) profiles of light transmission (solid line), methane (solid circles), ATP (open squares) (c), and trace metals (TDMn and TDFe) (d) from a vertical CTD casting (H05 CTD95). The locations of the paths and station are shown in Fig. 1c.

anomaly at H05 CTD95. The maximum concentration of methane was observed in the lower plume body at a depth of 1400 m, whereas ATP was highest in the upper plume body at a depth of 1200 m. The concentration of TDFe increased to a maximum of 148 nM at a depth of 1200 m and decreased slightly below 1200 m. Conversely, the concentration of TDMn increased with depth, with a maximum value at a depth of 1400 m, the lowest depth sampled.

Although Fe and Mn are the two metals most strongly enriched in hydrothermal vent fluids, they show contrasting behaviors when the fluids enter the ocean. Fe is readily removed from the fluids by the precipitation of Fe-sulfide phases at the venting site. The remaining Fe is oxidized over a longer time scale to Fe-oxyhydroxide particulate material within the buoyant plume (Chin *et al*., 1994; Lilley *et al*., 1995). In contrast, Mn does not readily form sulfide minerals and exhibits relatively sluggish oxidation kinetics. Oxidation of Mn from the vent is mediated by bacteria and increases with distance away from the vent field (Cowen *et al*., 1990). Therefore, Mn remains predominantly in the dissolved form within the hydrothermal plume near venting site (German and Von Damm, 2004). TDFe is highly enriched compared to TDMn in the plume at H05 CTD95, where Fe/Mn ratios vary from 16.2 to 40.2. The observed Fe/Mn ratios are significantly higher than those of typical midocean ridge plume (~1 to ~5, Von Damm, 1990) and those of the NELSC plume (1.2 to 1.7 at H06 CTD09). The lower concentration of TDFe at H05 CTD95 compared to those at the NELSC site (H06 CTD09) can be attributed to the distance from the venting source (Fig. 1).

The elevated Fe/Mn ratios in hydrothermal plume were also reported at the Kermadec volcanic arc (de Ronde *et al*., 2001) and Mariana volcanic arc (Resing *et al*., 2007). They attributed the elevated Fe/Mn ratios to the congruent dissolution of the host rock by highly acidic fluid (Resing and Sansone, 2002) or magmatic fluids. The presence of native sulfur recovered from the seafloor (see below), suggesting the degassing of magmatic SO_2 (i.e., a highly oxidized magmatic system). Therefore, the elevated Fe/Mn ratios at the MTJ-1 might be related to

magmatic fluids.

The contrasting vertical distributions of TDFe and TDMn observed at the H05 CTD95 casting indicate different sources. The upper plume signal at H05 CTD95, which is enriched in TDFe, CH_4, ATP, and less significantly TDMn, might be related to the plume from the central cone. Conversely, the lower plume signal, which is enriched in TDMn, CH_4, and less significantly TDFe (but not ATP), was observed at a lower depth compared with the plume signal at the central cone, and may therefore have originated from another source. Non-hydrothermal processes, such as suspended particles descending from the sea surface or the turbidity of bottom sediments caused by the towing devices touching the bottom, can be ruled out as causes of the weak light-transmission anomaly because such artificial anomalies would not be accompanied by chemical anomalies. Particle settling from beneath the dispersing plume or volcanic ash is a possible cause of the reduction in the plume signature at H05 CTD95, and may also be related to the decrease in ATP concentration; however, the increasing concentrations of CH_4 and TDMn within the lower plume signature suggest that other unknown sources, rather than the plume from the central cone, might affect the observed plume signature at H05 CTD95. The slight light-transmission anomaly observed near the second cone possibly indicates the source of a further discharge site (Fig. 5a).

At the MTJ-1 caldera, pieces of newly formed dacitic lava and hydrothermally altered rocks with fine-grained pyrite were sampled from the northeast flank of the central volcanic cone (Figs. 3e and f). The lava samples were composed of black lapilli, elemental sulfur infilling, and white material of an alunite and silica mixture, which is very similar to the volcanic lava from the Brimstone Pit of the active NW Rota-1 volcano in the Mariana Arc (Embley *et al*., 2006). The occurrence of native sulfur and alunite in the lava samples suggests the magmatic degassing of SO_2 and its disproportionation. The influence of magmatic degassing on the formation of hydrothermal systems has been proposed previously for several hydrothermal sites in arc and back-arc systems (Herzig *et al*., 1998; Kim *et al*., 2004; de Ronde *et al*., 2006). Although no plume signal was observed, altered dacitic rocks with pyrite grains (which may indicate extinct hydrothermal activity and mineralization) were also collected from the volcanic elevation of the northern caldera wall (Fig. 1).

The central volcanic cone is possibly a very young structure, as it displays a regular shape on the bathymetric map. The second cone, located southeast of the first, is less pronounced (Fig. 1). The occurrence of both cones indicates that this area could experience volcanic activity and a high heat flux, possibilities that are well supported by our observations. The northern part of the caldera wall contains a small depression, but small volcanic elevations were also observed (Fig. 1c). The light-transmission anomaly at the MTJ-1 was significantly stronger than those at other venting sites in the NE Lau Basin. However, the concentrations of other hydrothermal tracers at the MTJ-1 were not as great as light-transmission anomaly. Although we did not perform direct observation of the venting area or particle analysis of the plume, the presence of native sulfur and alunite in altered rock samples suggests that the plume at the MTJ-1 is probably formed by acid-sulfate type hydrothermal activity. If it is the case, the strong light-transmission anomaly would be attributed to formation of sulfur-rich particles as shown at the southern East Pacific Rise between 17°20′ and 18°40′ S (Feely *et al*., 1996). The precipitation of sulfur-rich particles might be occurred by release of large amount of magmatic gases possibly accompanied by magmatic input of fresh lava at the seafloor.

The discovery of vigorous hydrothermal and volcanic activity at the MTJ-1 caldera is new and interesting because there is no evidence of recent volcanic activity at other adjacent Tofua Arc volcanoes (Arculus, 2005). Arculus (2005) noted that the entire lengths of the FRSC and NELSC capture the total magmatic flux of the suprasubduction zone, possibly related to the shutting down of the adjacent Tofua Arc volcanoes. Thus, the MTJ-1 caldera, located between the NELSC and Tofua Arc, may provide valuable information on the interaction and/or intergradation between back-arc spreading and arc volcanism in the NE Lau Basin. German *et al*. (2006) suggested that the hydrothermal activity of the NELSC is a potential source of the regional-scale Tonga–Fiji plume in the Southwest Pacific (Lupton *et al*., 2004). The hydrothermal plume at the MTJ-1 caldera is too shallow to be the source of the 1750 m-centered regional Tonga–Fiji plume. However, the hydrothermal activity at the MTJ-1 can contribute to the regional accumulation of ^3He within the NE Lau Basin.

CONCLUSIONS

Our observations of extensive hydrothermal activity in back-arc spreading centers and an off-axis caldera within the NE Lau Basin are summarized as follow.

(1) We identified two active hydrothermal venting sites, one along the Fonualei Rift and Spreading Center (FRSC02 site) and the other at the southern summit of the Northeast Lau Spreading Center, based on investigations of temporal and spatial plume trends, including CTD tow-yo surveys and CTD castings, and by the recovery of a hydrothermal chimney. However, hydrothermal activity at the FRSC and NELSC cannot be fully explained in terms of two active venting sites: other potential venting sources should therefore be considered.

(2) The observation of strong, focused venting and the recovery of various volcanic eruptives at the central volcanic cone of the MTJ-1 caldera clearly indicate that the caldera hosts a major hydrothermal system. The occurrence of native sulfur and alunite indicates the degassing of magmatic SO_2, which suggests in turn an acid-sulfate type hydrothermal system. The elevated Fe/Mn ratios in hydrothermal plume at the MTJ-1, which is reported for several active seamounts at the Mariana and Kermadec volcanic arc, also might be related to magmatic fluids. The MTJ-1 caldera is noteworthy for its potential role as a link between active back-arc spreading and inactive arc volcanism in the NE Lau Basin, as well as another viable venting source that can contribute to the regional accumulation of ^{3}He in the NE Lau Basin.

Acknowledgments—We thank the crew of R/V *Onnuri* and scientists for their assistance during our cruises. We express our thanks to Drs. Martinez and Langmuir for providing bathymetric data and helpful comments for the preparation of our early cruise. We also thank S. R. Cho and K. T. Kim for analyzing methane and trace metal. S. J. Ju is thanks for his valuable comments on earlier draft of the manuscript. The careful reviews by two anonymous reviewers and associated editor (Dr. Ishibashi) substantially improved this contribution. This project was funded by the Ministry of Maritime Affairs and Fisheries of Korea (PM53101) and partly by Korea Ocean Research and Development Institute (PE9830R).

REFERENCES

Arculus, R. J. (2004) Voyage Summary SS11/2004: NoToVE-2004 (Northern Tonga Vents Expedition) Submarine hydrothermal plume activity and petrology of the northern Tofua Arc, Tonga. Available at http://www.marine.csiro.au/nationalfacility/voyagedocs/2004/Summary_SS11-2004.pdf

Arculus, R. J. (2005) Arc-backarc systems of northern Kermadec-Tonga. *Proceedings of 2005 New Zealand Minerals Conference*, 45–50.

Baker, E. T., Massoth, G. J., Nakamura, K., Embley, R. W., de Ronde, C. E. and Arculus, R. J. (2005) Hydrothermal activity on near-arc sections of back-arc ridges: Results from the Mariana Trough and Lau Basin. *Geochem. Geophys. Geosyst.* **6**, 2005GC000948.

Baker, E. T., Resing, J. A., Walker, S. L., Martinez, F., Taylor, B. and Nakamura, K. (2006) Abundant hydrothermal venting along melt-rich and melt-free ridge segments in the Lau back-arc basin. *Geophys. Res. Lett.* **33**, L07308.

Bloomer, S. H. and Wright, D. J. (1996) Summary of site survey cruise results, Boomerang Leg 08, in support of Proposal 451, Ocean Drilling in the Tonga Forearc: Subduction Geodynamics, Arc Evolution, and Deformation Processes at a Non-Accretionary Convergent Margin, Ocean Drilling Program Site Survey Data Bank, Palisades, New York.

Bulleid, N. C. (1978) An improved method for the extraction of Adenosine Triphosphate from marine sediment and seawater. *Limnol. Oceanogr.* **23**, 174–178.

Chin, C. S., Coale, K. H., Elrod, V. A., Johnson, K. S., Massoth, G. J. and Baker, E. T. (1994) *In situ* observations of dissolved iron and manganese in hydrothermal plumes, Juan de Fuca Ridge. *J. Geophys. Res.* **99**, 4969–4984.

Cowen, J. P., Massoth, G. J. and Baker, E. T. (1986) Bacterial scavenging of Mn and Fe in a mid- to far-field hydrothermal plume. *Nature* **322**, 169–171.

Cowen, J. P., Massoth, G. J. and Feely, R. A. (1990) Scavenging rates of dissolved manganese in a hydrothermal vent plume. *Deep-Sea Res.* **37**, 1619–1637.

de Ronde, C. E. J., Baker, E. T., Massoth, G. J., Lupton, J. E., Wright, I. C., Feely, R. A. and Greene, R. R. (2001) Intra-oceanic subduction-related hydrothermal venting, Kermadec volcanic arc, New Zealand. *Earth Planet. Sci. Lett.* **193**, 359–369.

de Ronde, C. E. J., Hannington, M., Stoffers, P., Wright, I., Ditchburn, R., Reyes, A., Baker, E., Massoth, G., Lupton, J., Walker, S., Greene, R., Soong, C., Ishibashi, J., Lebon, G., Bray, C. and Resing, J. (2006) Evolution of a submarine magmatic-hydrothermal system: Brother Volcano, Southern Kermadec Arc, New Zealand. *Econ. Geol.* **100**, 1097–1133.

Embley, R., Chadwick, W., Baker, E., Dutterfield, D., Resing, J., de Ronde, C., Tunnicliffe, V., Lupton, J., Juniper, S., Rubin, K., Stern, R., Lebon, G., Nakamura, K., Merle, S., Hein, J., Wiens, D. and Tamura, Y. (2006) Long-term eruptive activity at a submarine arc volcano. *Nature* **441**, 494–497.

Feely, R. A., Baker, E. T., Marumo, K., Urabe, T., Ishibashi, J., Gendron, J., Lebon, G. T. and Okamura, K. (1996) Hydrothermal plume particles and dissolved phosphate over the superfast-spreading southern East Pacific Rise. *Geochim. Cosmochim. Acta* **60**, 2297–2323.

Fouquet, Y., Steckelberg, U., Charlou, J., Donval, J., Foucher, J., Erzinger, J., Herzig, P., Muhe, R., Weidicke, M., Soakai, S. and Whitechurch, H. (1991) Hydrothermal activity in the Lau back-arc basin: Sulfides and water chemistry. *Geology* **19**, 303–306.

German, C. R. and Von Damm, K. L. (2004) Hydrothermal processes: Treatise on geochemistry, vol. 6. *The Oceans and Marine Geochemistry* (Turekian, K. K. and Holland, H. D., eds.), 181–222, Elsevier, Oxford.

German, C. R., Baker, E. T., Connelly, D. P., Lupton, J. E., Resing, J., Prien, R. D., Walker, S. L., Edmonds, H. N. and Langmuir, C. H. (2006) Hydrothermal exploration of the Fonualei Rift and Spreading Center and the Northeast Lau Spreading Center. *Geochem. Geophys. Geosyst.* **7**, 2006GC001324.

Hawkins, J. W. (1995) The geology of the lau basin. *Backarc Basins: Tectonics and Magmatisms* (Taylor, B., ed.), 63–138, Plenum, New York.

Herzig, P. M., Hannington, M. D., Fouquet, Y., von Stackelberg, U. and Petersen, S. (1993) Gold-rich polymetallic sulfides from the Lau back arc and implications for the geochemistry of gold in seafloor hydrothermal systems of the Southwest Pacific. *Econ. Geol.* **88**, 2178–2205.

Herzig, P. M., Hannington, M. D. and Arribas, A., Jr. (1998) Sulfur isotopic composition of hydrothermal precipitates from the Lau back-arc: implications for magmatic contri-

butions to seafloor hydrothermal systems. *Mineralium Deposita* **33**, 226–237.

Kim, J., Lee, I. and Lee, K. Y. (2004) S, Sr, and Pb isotopic systematics of hydrothermal chimney precipitates from the Eastern Manus Basin, western Pacific: evaluation of magmatic contribution to hydrothermal system. *J. Geophys. Res.* **107**, B12210.

Kim, J., Lee, I., Halbach, P., Lee, K. Y., Ko, Y. T. and Kim, K. H. (2006a) Formation of hydrothermal vents in the North Fiji Basin: Sulfur and lead isotope constraints. *Chem. Geol.* **233**, 257–275.

Kim, J., Lee, K. Y., Hyeong, K., Moon, J. W. and Shipboard Scientific Party (2006b) Discovery of hydrothermal activities in the Fonualei Rift and Spreading Center (FRSC) in the Lau Basin (abstract). *Minerals of the Ocean-3 Future Developments Abstracts*, p. 68.

Kim, J., Ko, Y. T., Son, S. K. and Lee, K. Y. (2007) Hydrothermal activity in back-arc and arc caldera in the NE Lau Basin (abstract). *Spring Meeting of Geological Sciences of Korea, Abstract with Program*, p. 486–488.

Lilley, M. D., Feely, R. A. and Trefry, J. H. (1995) Chemical and biochemical transformations in hydrothermal plumes. *Geophysical Monograph 91, Seafloor Hydrothermal Systems: Physical, Chemical, Biological, and Geological Interactions* (Humphris, S. E. *et al*., eds.), 369–391, American Geophysical Union, Washington, D.C.

Lupton, J. E., Pyle, D. G., Jenkins, W. J., Greene, R. and Evans, L. (2004) Evidence for an extensive hydrothermal plume in the Tonga–Fiji region of the South Pacific. *Geochem. Geophys. Geosyst.* **5**, 2003GC000607.

Martinez, F. and Taylor, B. (2006) Modes of crustal accretion in back-arc basins: Inferences from the Lau Basin. *Back-arc Spreading Systems: Geological, Biological, Chemical, and Physical Interactions* (Christie, D. M. *et al*., eds.), *Geophysical Monograph* **166**, 5–30, American Geophysical Union, Washington, D.C.

Martinez, F., Taylor, B., Baker, E. T., Resing, J. A. and Walker, S. L. (2006) Opposing trends in crustal thickness and spreading rate along the back-arc Eastern Lau Spreading Center: Implications for controls on ridge morphology, faulting, and hydrothermal activity. *Earth Planet. Sci. Lett.* **245**, 655–672.

Ohta, K., Terai, H., Kimura, I. and Tanaka, K. (1999) Simultaneous determination of hydrogen, methane, and carbon monoxide in water by gas chromatography with a semiconductor detector. *Anal. Chem.* **71**, 2697–22699.

Resing, J. A. and Sansone, F. J. (2002) The chemistry of lava-seawater interactions II: The elemental signature. *Geochim. Cosmochim. Acta* **66**, 1925–1941.

Resing, J. A., Lebon, G., Baker, E. T., Lupton, J. E., Embley, R. W., Massoth, G. J., Chadwick, W. W. and de Ronde, C. E. J. (2007) Venting of acid-sulfate fluids in a high sulfidation setting at NW Rota-1 submarine volcano on the Mariana Arc. *Econ. Geol.* **102**, 1047–1061.

Statham, P. J. (1985) The determination of dissolved manganese and cadimium in sea water at low nmol l^{-1} concentrations by chelation and extraction followed by electrothermal atomic absorption spectrometry. *Anal. Chim. Acta* **169**, 145–159.

Von Damm, K. L. (1990) Seafloor hydrothermal activity: Black smoker chemistry and chimneys. *Annu. Rev. Earth Planet. Sci.* **18**, 173–204.

Walker, S. L., Baker, E. T., Massoth, G. J. and Hey, R. N. (2004) Short-term vatiations in the distribution of hydrothermal plumes along a superfast spreading center, East Pacific Rise, 27°30′–32°20′ S. *Geochem. Geophys. Geosyst.* **5**, 2004GC000789.

Webster, J. J., Hampton, G. J. and Leach, F. R. (1984) ATP in soil: a new extractant and extraction procedure. *Soil. Biol. Biochem.* **16**, 335–342.

Winn, C. D., Karl, D. M. and Massoth, G. J. (1986) Microorganisms in deep-sea hydrothermal plumes. *Nature* **320**, 744–746.

Zellmer, K. E. and Taylor, B. (2001) A three-plate kinematic model for Lau Basin opening. *Geochem. Geophys. Geosyst.* **2**, 2000GC000106.